

## Journal Pre-proof

Exploring the detailed spectroscopic characteristics, chemical and biological activity of two cyanopyrazine-2-carboxamide derivatives using experimental and theoretical tools

Shargina Beegum, Y. Sheena Mary, Y. Shyma Mary, Renjith Thomas, Stevan Armarković, Sanja J. Armarković, Jan Zitko, Martin Dolezal, C. Van Alsenoy



PII: S1386-1425(19)30804-2

DOI: <https://doi.org/10.1016/j.saa.2019.117414>

Reference: SAA 117414

To appear in: *Spectrochimica Acta Part A: Molecular and Biomolecular Spectroscopy*

Received date: 24 June 2019

Revised date: 13 July 2019

Accepted date: 21 July 2019

Please cite this article as: S. Beegum, Y.S. Mary, Y.S. Mary, et al., Exploring the detailed spectroscopic characteristics, chemical and biological activity of two cyanopyrazine-2-carboxamide derivatives using experimental and theoretical tools, *Spectrochimica Acta Part A: Molecular and Biomolecular Spectroscopy*(2019), <https://doi.org/10.1016/j.saa.2019.117414>

This is a PDF file of an article that has undergone enhancements after acceptance, such as the addition of a cover page and metadata, and formatting for readability, but it is not yet the definitive version of record. This version will undergo additional copyediting, typesetting and review before it is published in its final form, but we are providing this version to give early visibility of the article. Please note that, during the production process, errors may be discovered which could affect the content, and all legal disclaimers that apply to the journal pertain.



Exploring the detailed spectroscopic characteristics, chemical and biological activity of two cyanopyrazine-2-carboxamide derivatives using experimental and theoretical tools

Shargina Beegum<sup>a</sup>, Y.Sheena Mary<sup>a</sup>, Y.Shyma Mary<sup>a</sup>, Renjith Thomas<sup>b\*</sup>, Stevan Armaković<sup>c</sup>, Sanja J. Armaković<sup>d</sup>, Jan Zitko<sup>e</sup>, Martin Dolezal<sup>e</sup>, C. Van Alsenoy<sup>f</sup>

<sup>a</sup> Department of Physics, Fatima Mata National College, Kollam, Kerala, India

<sup>b</sup> Department of Chemistry, St Berchmans College (Autonomous), Changanassery, Kerala, India 686101

<sup>c</sup> University of Novi Sad, Faculty of Sciences, Department of Physics, Trg D. Obradovića 4, 21000 Novi Sad, Serbia

<sup>d</sup> University of Novi Sad, Faculty of Sciences, Department of Chemistry, Biochemistry and Environmental Protection, Trg D. Obradovića 3, 21000 Novi Sad, Serbia

<sup>e</sup> Faculty of Pharmacy in Hradec Kralove, Charles University in Prague, Heyrovskeho 1203, Hradec Kralove, 500 05, Czech Republic

<sup>f</sup> Department of Chemistry, University of Antwerp, Groenenborgerlaan 171, B-2020, Antwerp, Belgium

\*author for correspondence: renjith@sbcollege.ac.in

## Abstract

This article represents the spectroscopic and computational studies of two new pyrazine compounds. In order to establish the structure and functional nature of the compounds, we have employed fourier transformed infrared (FT-IR) and Raman spectra, nuclear magnetic resonance (NMR) spectra, and ultraviolet (UV) absorptions and have compared them with the simulated computational spectra and found that they are in the agreeable range. Simulated hyperpolarisability values are used to obtain the nonlinear optic (NLO) activity of the compound, to be used in organic electronic materials. The charge transfer and related properties was investigated by the simulation of electronic spectrum with time dependent density functional theory (TD-DFT). Natural transition orbitals (NTO) provides information about which region of the molecules are more involved in the electronic transitions and the charge transfer properties for the lowest energy excitation have been analyzed on the basis of electron density variation.

Molecular dynamics simulations provides information about the behavior of the molecule in solutions. frontier orbital analysis and study of various reactivity rdescriptors like ALIE and fukui provided deep knowledge on the reactivity side. Molecular docking has been also performed to investigate the interaction between title molecules and exhibits inhibitory activity against *Pseudomonas aeruginosa*Enoyl-Acyl carrier protein reductase (FabI).

**Keywords:** DFT; ALIE; RDF; Carboxamide; Docking; BDE.

## 1. Introduction

Pyrazine is an important heterocyclic aromatic compound of biological and industrial significance that occur in nature and may be synthesized in numerous ways. Its derivatives are well known and important and contain two nitrogen atoms in its aromatic ring and can carry substituent at one or more of the four ring carbon atoms. Nitrogen containing hetrocyclici compounds find high applications in drug industry as well as agriculture in the form of insect repllents[1]. Some bacteria can use pyrazine derivatives as a source of subsistence energy [2]. Substituted pyrazines are present in many of the food forms like meat, poultry products, protein containing vegetables etc [3]. Tetramethylpyrazine, called as ligustrazine is present in some Chinese natural herbs, which could act as antioxidants to scavenge dangerous free radicals [4]. Tuberculosis, a deadly infectious disease now is taking many drug resistant forms, and is making the treatment and management very difficult. Hence new antibacterial agents are required to combat the drug resistant TB infections [5]. Pyrazinamide is an important anti TB agent used as a first line agent for tuberculosis therapy [6] and even it can be fatal to semidormant mycobacteria [7]. Aminopyrazine have been reported to be inhibitor of MK-2 which plays a critical role in regulating TNF $\alpha$ , a cytokine that is over produced in several inflammatory diseases like rheumatoid arthritis [8] and some of its derivatives are used for the treatment of glaucoma [9]. Theyshows various types of pharmacological activities like antibacterial, antifungal, antiviral, anti-oxidant and anti-cancer activities [10,11] and also pyrazinamides and pyrazine sulphonamides have been used on various topics as oral anti-diabetics, nutrition supplement, insecticides and fungicides [1]. Pyrazines are also anthropogenic, especially dihydropyrazines and are vital for almost all forms of life due to its ability to intercalate DNA by

affecting the process of apoptosis [12]. Pyrazines are well established to act as exo-bidentate ligands [13] and besides their medicinal uses, pyrazines have found technical applications in several organic electronics applications [14]. Pyrazines have been intensively investigated as effective corrosion inhibitors in different acid medium [15-17].

The present study performs a detailed analysis of experimental and simulated spectra of the two cyanopyrazine-2-carboxamide derivatives, 5-cyano-3-((4-methoxybenzyl)amino)pyrazine-2-carboxamide (CMOBAPC) and 5-cyano-3-((4-methylbenzyl)amino)pyrazine-2-carboxamide (CMBAPC). FT-IR, FT-Raman, frontier molecular orbital analysis, natural bond orbital analysis, non-linear optical properties and molecular electrostatic potential study are reported. The biological activities of the compounds are predicted by molecular docking study. In this study we consider title molecules as possibly suitable for application in pharmaceutical industry. In case they are found in pharmaceutical formulations they could produce certain damage to the environment [18-23], once they are dumped into some type of water. Therefore in this study we were also motivated to assess their degradation properties based on DFT calculations and MD simulations. Modern techniques for the removal of pharmaceutical waste are based on oxidation, which induces degradation [24]. Autoxidation tendency of a molecule is in correlation with bond dissociation energies for abstraction of hydrogen atoms (H-BDE) [25-28]. DFT calculations are widely used in environmental studies [29] and the concept of H-BDE allows employment of DFT calculations for inexpensive assessment of degradation properties as well. Stability in water is also very important for the removal of pharmaceutical waste and for which MD analysis are of great importance, as they enable one to explicitly include solvent molecules and to identify which atoms have significant interactions with solvent. In the same time we have performed detailed TD-DFT calculations in order to see information into the charge transfer properties of the lowest energy excitation.

## 2. Experimental details- Spectral analysis

The title compounds (see Fig.1) can be easily synthesized by homolytic amidation of commercially available 6-chloropyrazine-2-carbonitrile (**1**) to resulting 3-chloro-5-cyanopyrazine-2-carboxamide (**2**), which subsequently undergoes nucleophilic substitution of chlorine by corresponding benzylamine (Scheme 1). The amino dehalogenation reaction utilizes

potassium carbonate as a base and proceeds at RT to completion in approximately 1 hour (checked by TLC). The identity of compounds was assessed by  $^1\text{H}$  and  $^{13}\text{C}$  NMR spectra and melting point determination. The results were fully consistent with the declared structures.

NMR spectra of the compounds were obtained using Varian VNMR S500 at 500 MHz for  $^1\text{H}$ -NMR and 125 MHz for  $^{13}\text{C}$ -NMR using  $\text{DMSO-}d_6$  and the chemical shift is measured using TMS as the reference. The FT-IR spectra (Fig.S1-supporting information) and FT-Raman spectra (Fig.S2- supporting information) were analysed using a DR/Jasco FT-IR 6300 and Bruker RFS 100/s spectrometer. Element analysis were done with on EA-1110 CHN analyser. UV-VIS spectra were measured in methanolic solution, where the concentrations of title compounds were approximately  $1.10^{-4}$  mol/L. Methanol (CHROMASOLV®, for HPLC,  $\geq 99.9\%$ , Sigma-Aldrich, Germany) was used as a solvent and a blank sample. The spectra were recorded on UV-2600 UV-VIS spectrophotometer in the range 200–600 nm, the path length of the cuvette was 10 mm.

### 3. Computational details

Computational simulations related to this paper was performed by a variety of softwares. The molecules were optimised using Gaussian09 program [30] employing the generic B3LYP functional along with CC-pVDZ (5D, 7F) basis set to reach an optimised geometry. Frequency calculations were also performed to make sure that there are no imaginary frequencies to confirm the minimal structure. The IR spectra generated was used to analyse the fundamental modes; but they have been overestimated by the DFT hybrid B3LYP functional, hence a scaling factor of 0.9613 had to be used in order to make it in accordance with the experimental data [31]. The wave number assignments were performed using Gaussview [32] and GAR2PED software packages [33]. Simulated structure of the compounds CMBAPC and CMOBAPC are provided in Fig. 1 and geometric parameters are provided in the Table S1 (supporting information).

Some features of the Schrödinger Materials Science Suite 2017-4 [34] like Jaguar [35-37] and Desmond [38-41] were used to do some specialised DFT studies and molecular dynamics simulations. In Jaguar also, B3LYP functional[42] along with 6-311++G(d,p), 6-31+G(d,p) and 6-311G(d,p) basis sets were used for Average Local Ionisation Energy (ALIE), Fukui functions and Bond Dissociation Energies (BDE), respectively. CAM-B3LYP [43] functional was used to do time dependent density functional theory calculations (TD-DFT) along with 6-31+G(d,p) basis sets to simulate the electronic spectra [44]. For MD simulations OPLS 3 force field [38,

45-47] was used, with cut off radius to 12 Å, simulation time 10 ns, temperature to 300 K and pressure to 1.0325 bar. For solvent atmosphere, simple point charge (SPC) [48] approach was used and the molecules are placed in a cage of about 3000 water molecules. Electron density analysis employing the method developed by Johnson et al was used to study the intra-molecular noncovalent interactions [49, 50]. Maestro GUI [51] was used for the preparation of input files when Schrödinger Materials Science Suite 2017-1 was used. Multiwfn [52-55] program for the analysis of wave function was used for the investigation of charge transfer due to the excitation. Electron density variation was visualized with the aid of VMD program [56-62], while Tachyon [63] was used for rendering of figures.

## 4. Results and discussion

### 4.1 Geometrical Parameters

In the present case the pyrazine bond lengths C<sub>1</sub>-C<sub>2</sub>, C<sub>2</sub>-N<sub>3</sub>, N<sub>3</sub>-C<sub>4</sub>, C<sub>4</sub>-C<sub>5</sub>, C<sub>5</sub>-N<sub>6</sub>, N<sub>6</sub>-C<sub>1</sub> are 1.4026, 1.337, 1.3305, 1.4424, 1.3512, 1.336 Å for CMBAPC and 1.4026, 1.3371, 1.3304, 1.443, 1.3516, 1.3358 Å for CMOBAPC respectively. For a similar derivative the reported values are 1.4060, 1.3580, 1.3260, 1.4370, 1.3600 and 1.354 Å [64]. The CN bond length in the pyrazine rings of CMBAPC and CMOBAPC are much lesser than normal C-N single bond which is 1.49 Å [65]. The two C-C bond lengths of pyrazine are also smaller than that of normal C-C single bond of 1.54 Å [66]. The C=O bond lengths for CMBAPC is 1.2364 Å and for CMOBAPC is 1.2362 Å whereas the reported values are 1.2253 Å, 1.2203 Å and 1.2123 Å [67]. The bond lengths C<sub>5</sub>-N<sub>10</sub> and C<sub>11</sub>-N<sub>10</sub> are 1.3475 and 1.457 Å for CMBAPC and it is 1.3469 and 1.4598 Å for CMOBAPC. The C<sub>28</sub>-N<sub>30</sub> bond length for CMBAPC and C<sub>24</sub>-N<sub>26</sub> bond length for CMOBAPC are 1.3518 Å and 1.352 Å respectively which is shorter than the normal CN single bond length 1.49 Å and hence these bonds can be confirmed to have some double bond or conjugate bond character [68]. The variation in the C=O and CN bond lengths are congruous with the inference that the hydrogen bond decreases its double bond characteristics [69]. For CMBAPC and CMOBAPC the bond angles at C<sub>1</sub> position, C<sub>2</sub>-C<sub>1</sub>-C<sub>8</sub>, C<sub>2</sub>-C<sub>1</sub>-N<sub>6</sub>, N<sub>6</sub>-C<sub>1</sub>-C<sub>8</sub> are 119.4, 123.4, 117.2° respectively. This indicates the interaction between the pyrazine ring and C≡N. The C<sub>8</sub>≡N<sub>9</sub> bond length in CMBAPC and CMOBAPC is 1.163 Å. At C<sub>4</sub> position, for CMBAPC the bond angles C<sub>5</sub>-C<sub>4</sub>-C<sub>28</sub>, N<sub>3</sub>-C<sub>4</sub>-C<sub>5</sub>, N<sub>3</sub>-C<sub>4</sub>-C<sub>28</sub> and for CMOBAPC the bond angles C<sub>5</sub>-C<sub>4</sub>-C<sub>24</sub>, N<sub>3</sub>-C<sub>4</sub>-C<sub>5</sub>, N<sub>3</sub>-C<sub>4</sub>-C<sub>24</sub> are 121.6, 121.2, 117.2° respectively which shows the

interaction between the pyrazine ring and C=ONH<sub>2</sub>. At C<sub>5</sub> position the bond angles for CMBAPC and CMOBAPC, C<sub>4</sub>-C<sub>5</sub>-N<sub>6</sub>, C<sub>4</sub>-C<sub>5</sub>-N<sub>10</sub>, N<sub>6</sub>-C<sub>5</sub>-N<sub>10</sub> are 119.7, 121.6, 118.6° and 119.7, 121.6, 118.7° respectively. The interaction between pyrazine and NH bond is the main reason for the asymmetry. At N<sub>10</sub> position, for CMBAPC, the angles C<sub>5</sub>-N<sub>10</sub>-H<sub>33</sub>, C<sub>11</sub>-N<sub>10</sub>-H<sub>33</sub>, C<sub>5</sub>-N<sub>10</sub>-C<sub>11</sub> are 114.5, 120.9, 124.3° and for CMOBAPC the angles C<sub>5</sub>-N<sub>10</sub>-H<sub>34</sub>, C<sub>11</sub>-N<sub>10</sub>-H<sub>34</sub>, C<sub>5</sub>-N<sub>10</sub>-C<sub>11</sub> are 114.6, 120.7, 124.5° respectively and the asymmetry of the angles at this position indicates the interaction of NH with neighboring units [70, 71]. At C<sub>12</sub> position, the bond angles C<sub>11</sub>-C<sub>12</sub>-C<sub>13</sub>, C<sub>11</sub>-C<sub>12</sub>-C<sub>14</sub>, C<sub>13</sub>-C<sub>12</sub>-C<sub>14</sub> for CMBAPC and CMOBAPC are 120.5, 121.4, 118.2° and 120.9, 121.1, 118.0° respectively and this asymmetry shows the interaction between phenyl ring and CH<sub>2</sub> group. At C<sub>19</sub> position, the bond angles for CMBAPC, C<sub>15</sub>-C<sub>19</sub>-C<sub>24</sub>, C<sub>17</sub>-C<sub>19</sub>-C<sub>24</sub>, C<sub>15</sub>-C<sub>19</sub>-C<sub>17</sub> are 121.6, 120.7, 117.7° and for CMOBAPC, the bond angles C<sub>15</sub>-C<sub>19</sub>-O<sub>29</sub>, C<sub>17</sub>-C<sub>19</sub>-O<sub>29</sub>, C<sub>15</sub>-C<sub>19</sub>-C<sub>17</sub> are 115.7, 125.0, 119.4° respectively which shows the interaction of the phenyl ring with the CH<sub>3</sub> group for CMBAPC and -OCH<sub>3</sub> group of CMOBAPC. The C-C bond lengths in the phenyl ring lies in the range 1.3939-1.4053 Å for CMBAPC and in the range 1.3887-1.4075 Å for CMOBAPC. The reported values of C-C bond length for benzene is 1.3993 Å [72] and for benzaldehyde is 1.3973 Å [73].

## 4.2 IR and Raman spectra

The experimental IR and Raman spectral data, was compared with the scaled simulated spectra and are represented in Table 1. The potential energy distribution and assignments of the vibrational modes are also included in the table. The phenyl and pyrazine rings are represented by the letters Ph and Pz respectively. νC=O modes are assigned at 1682 cm<sup>-1</sup> theoretically, 1688 cm<sup>-1</sup> (IR), 1681 cm<sup>-1</sup> (Raman) for CMBAPC and at 1682 cm<sup>-1</sup> theoretically, 1686 cm<sup>-1</sup> (IR), 1684 cm<sup>-1</sup> (Raman) for CMOBAPC as expected. The C=O stretching has a PED of 60% for both CMBAPC and CMOBAPC with IR Intensity 419.40, 410.17 and Raman activity 37.67, 38.90 respectively. The NH<sub>2</sub> stretching give rise to bands at 3450-3150 cm<sup>-1</sup> and its deformations, rocking, twisting and wagging modes are expected in the range 1640-1580 cm<sup>-1</sup>, 1170-1080 cm<sup>-1</sup>, 820-730 cm<sup>-1</sup> and 730-610 cm<sup>-1</sup> respectively [74-77]. The NH<sub>2</sub> stretching modes are assigned at 3447 cm<sup>-1</sup> (IR), 3578, 3423 cm<sup>-1</sup> (Raman), 3572, 3425 cm<sup>-1</sup> (DFT) for CMBAPC and at 3389 cm<sup>-1</sup> (IR), 3436 cm<sup>-1</sup> (Raman), 3573, 3425 cm<sup>-1</sup> (DFT) for CMOBAPC. For the modes at 3572 and 3425 cm<sup>-1</sup> the IR intensities are 87.73 and 63.06 and Raman activities are 84.99 and 163.74 for

CMBAPC with a PED of 99%. For CMOBAPC the modes at 3573 and 3425  $\text{cm}^{-1}$  have IR intensities 87.07 and 62.16 and Raman activities 85.08 and 163.38 and PED of 99%.

The  $\text{NH}_2$  deformation are seen at 1501, 1050, 605, 603  $\text{cm}^{-1}$  (DFT), 1506, 601  $\text{cm}^{-1}$  (IR), 1506, 601  $\text{cm}^{-1}$  (Raman) for CMBAPC with PEDs of 61%, 50%, 58%, 44% respectively and at 1501, 1050, 605, 602  $\text{cm}^{-1}$  (DFT), 1505, 1055, 601  $\text{cm}^{-1}$  (IR), 1504, 1057, 603  $\text{cm}^{-1}$  (Raman) for CMOBAPC with 61%, 54%, 59% and 47% PEDs respectively. The IR and Raman of these modes for CMBAPC are 236.50, 0.26, 3.20, 4.58 and 17.10, 29.27, 3.71 and 4.46 and for CMOBAPC they are 235.36, 0.37, 5.32, 7.31 and 17.75, 29.20, 4.17, and 4.63 respectively. NH stretching, in-plane and out-of-plane bending modes are assigned at 3293, 1305, 693  $\text{cm}^{-1}$  (DFT), 3259, 1303, 693  $\text{cm}^{-1}$  (IR), 3293, 1308, 693  $\text{cm}^{-1}$  (Raman) for CMBAPC and for CMOBAPC these modes are at 3296, 1571, 690  $\text{cm}^{-1}$  (DFT), 3297, 1574, 692  $\text{cm}^{-1}$  (IR), 3294, 1570, 693  $\text{cm}^{-1}$  (Raman) respectively which is in good agreement with the expected values. The N-H stretching mode has a PED of 99% with IR intensities 187.24 (CMBAPC), 186.93 (CMOBAPC) and Raman activities 132.77 (CMBAPC), 129.67 (CMOBAPC). The PED of the N-H deformation modes are 49% and 43% for CMBAPC and 43% and 39% for CMOBAPC. Deformation mode at 1305  $\text{cm}^{-1}$ , the IR and Raman are respectively 24.29 and 25.89 and for the mode at 693  $\text{cm}^{-1}$ , the IR intensity and Raman activity are 41.29 and 1.12 for CMBAPC. For the deformation mode at 1571  $\text{cm}^{-1}$  for CMOBAPC the IR intensity and Raman activity are respectively 524.17 and 13.59 and for the mode at 690  $\text{cm}^{-1}$ , the IR intensity and Raman activity are 53.45 and 0.79. The CN stretching modes are observed at 1045  $\text{cm}^{-1}$  (IR), 1097, 1039  $\text{cm}^{-1}$  (Raman), 1098, 1034, 1050  $\text{cm}^{-1}$  (DFT) for CMBAPC with IR intensities 2.07, 4.18, 0.26, Raman activities 28.77, 2.35, 29.27 and PED 41%, 45% and 39% respectively and at 1055, 1096, 1027  $\text{cm}^{-1}$  (IR), 1057, 1031  $\text{cm}^{-1}$  (Raman), 1050, 1094, 1029  $\text{cm}^{-1}$  for CMOBAPC with IR intensities 0.37, 4.11, 26.45, Raman activities 29.20, 33.21, 3.89 and PED 38%, 44%, and 37% respectively and the expected range for these modes are 1100-1300  $\text{cm}^{-1}$  [74-77].

The  $\text{CH}_2$  stretching and deformation modes are assigned at 2865, 1332, 1184  $\text{cm}^{-1}$  (IR), 2887, 1333, 1283, 1194  $\text{cm}^{-1}$  (Raman), 2963, 2893, 1421, 1331, 1283, 1199  $\text{cm}^{-1}$  (DFT) for CMBAPC and at 2970, 1284  $\text{cm}^{-1}$  (IR), 2970, 2893, 1338, 1284  $\text{cm}^{-1}$  (Raman), 2972, 2895, 1423, 1334, 1286, 1195  $\text{cm}^{-1}$  (DFT) for CMOBAPC where the expected range is 2900-3100  $\text{cm}^{-1}$  for  $\text{CH}_2$  stretching and 800-1500  $\text{cm}^{-1}$  for deformations [74]. For CMBAPC the stretching mode at

2963  $\text{cm}^{-1}$  has a PED of 99% with IR intensity of 6.01 and Raman activity of 86.45 and the mode at 2893  $\text{cm}^{-1}$  has a PED of 100% with IR of 38.66 and Raman of 165.32. For the deformation modes at 1421, 1331, 1283 and 1199  $\text{cm}^{-1}$  the IR intensities are 25.63, 56.17, 19.32 and 30.92 and Raman activities are 11.21, 16.63, 23.18 and 33.34 and the PEDs are 90, 68, 42 and 63%. For CMOBAPC the stretching modes at 2972, 2895  $\text{cm}^{-1}$  have 100% PED with IR intensities 5.03, 41.13 and Raman activities 80.46 and 165.77. The deformation modes of CMOBAPC have IR intensities of 10.40, 116.61, 28.39, 63.24 and Raman activities of 11.82, 27.09, 39.47, 22.38 with PEDs 85, 64, 69 and 62%. The  $\text{CH}_3$  stretching and deformation modes for CMBAPC are assigned at 1402, 1019  $\text{cm}^{-1}$  (IR), 2994, 2968, 2905, 1412, 1381, 1012  $\text{cm}^{-1}$  (Raman), 2995, 2966, 2910, 1414, 1399, 1381, 1342, 1010  $\text{cm}^{-1}$  (DFT) with a PED of 100% for the modes at 2995, 2966  $\text{cm}^{-1}$  and also the IR intensities are 15.00, 15.73 and Raman activities are 72.42 and 113.79 whereas for the mode at 2910  $\text{cm}^{-1}$  has a PED of 60% with 34.86 IR intensity and 278.30 Raman activity. And for CMOBAPC these modes are assigned at 3020, 2944, 1408, 1117  $\text{cm}^{-1}$  (IR), 3020, 2940, 2880  $\text{cm}^{-1}$  (Raman), 3017, 2948, 2885, 1421, 1405, 1403, 1149, 1114  $\text{cm}^{-1}$  (DFT). The PED for the modes at 3017  $\text{cm}^{-1}$  is 91% with IR intensity 23.03 and Raman activity 158.71. For the modes at 2948 and 2885  $\text{cm}^{-1}$  the PED is 100% with IR intensities 39.51 and 63.28 and Raman activities of 70.81 and 163.05. All these modes are in accordance with the expected range 2860-3000  $\text{cm}^{-1}$  (stretching) and the 1365-1485  $\text{cm}^{-1}$  (deformations) [74].

The  $\text{C}\equiv\text{N}$  stretching mode indicates absorption at 2200-2280  $\text{cm}^{-1}$  [74, 78]. In the present case the  $\text{C}\equiv\text{N}$  stretching vibration is assigned at 2238  $\text{cm}^{-1}$  (IR), 2262  $\text{cm}^{-1}$  (Raman), 2257  $\text{cm}^{-1}$  (DFT) with low IR 2.19 and a high Raman 536.23 for CMBAPC and at 2245  $\text{cm}^{-1}$  (IR), 2247  $\text{cm}^{-1}$  (Raman), 2257  $\text{cm}^{-1}$  (DFT) with low IR 2.39 and a high Raman 541.06 for CMOBAPC with a PED of 89% for both the compounds.

C-C stretching are found theoretically at 1188, 1183  $\text{cm}^{-1}$  for CMBAPC with IR intensities 6.80, 9.40 and Raman activities 16.94, 19.85 and PEDs of 44% and 40%. For CMOBAPC, C-C stretching band is observed at 1184  $\text{cm}^{-1}$  theoretically. These bands are not observed in the IR and Raman. The PED for this band is 41% with IR intensity 9.86 and Raman activity 30.34.

CH stretching modes of the pyrazine ring are usually in the range of 3000-3100  $\text{cm}^{-1}$  [65] and for these molecules, they are assigned at 3076  $\text{cm}^{-1}$  (DFT), 3088  $\text{cm}^{-1}$  (IR), 3080  $\text{cm}^{-1}$

(Raman) with low IR intensity of 3.50 and Raman activity of 148.33 for CMBAPC and at 3076  $\text{cm}^{-1}$  with low IR intensity of 3.59 and Raman activity of 150.20 for CMOBAPC theoretically and 99% PED for both the title compounds. The pyrazine ring stretching modes are at 1530, 1424, 1234  $\text{cm}^{-1}$  in the IR, 1533, 1435, 1230  $\text{cm}^{-1}$  in the Raman, 1523-1228  $\text{cm}^{-1}$  theoretically for CMBAPC and at 1527, 1434, 1260,  $\text{cm}^{-1}$  in the IR spectrum, 1525, 1437, 1260  $\text{cm}^{-1}$  in the Raman spectrum, 1522-1228  $\text{cm}^{-1}$  with theoretically for CMOBAPC. For CMBAPC and CMOBAPC the PEDs are in the range 58-50%. The modes at 1523 and 1228  $\text{cm}^{-1}$  for CMBAPC have IR intensities 118.40 and 28.24 and have Raman activities 210.73 and 9.07. For CMOBAPC the modes at 1522 and 1228  $\text{cm}^{-1}$  have IR intensities of 112.89 and 27.78 and Raman activities of 211.96 and 8.73. The ring breathing modes of CMBAPC and CMOBAPC are assigned at 1097  $\text{cm}^{-1}$  (Raman), 1098  $\text{cm}^{-1}$  (DFT) and 1096  $\text{cm}^{-1}$  (IR), 1094  $\text{cm}^{-1}$  (DFT) respectively. The mode is having a very low IR intensity of 2.07, Raman activity of 28.77 and a PED of 48% for CMBAPC and for CMOBAPC the IR intensity is low (4.11) with Raman activity 33.21 and PED 46%. The CH deformation modes of the pyrazine ring are assigned at 1424  $\text{cm}^{-1}$  (IR), 1435  $\text{cm}^{-1}$  (Raman), 1434  $\text{cm}^{-1}$  (DFT) with IR intensity 11.97, Raman activity 15.29 and the PED is 44%, 844  $\text{cm}^{-1}$  (Raman), 848  $\text{cm}^{-1}$  (DFT) with IR intensity 9.40, Raman activity 0.28 and the PED is 82% for CMBAPC and 1434  $\text{cm}^{-1}$  (IR), 1437  $\text{cm}^{-1}$  (Raman), 1434  $\text{cm}^{-1}$  (DFT) with IR intensity 10.92, Raman activity 16.74 and the PED is 44% 847  $\text{cm}^{-1}$  (DFT) with IR intensity 9.22, Raman activity 0.29 and the PED is 82% for CMOBAPC.

The phenyl CH stretching modes for CMBAPC and CMOBAPC are assigned at 3051, 3021  $\text{cm}^{-1}$  (IR), 3057, 3037  $\text{cm}^{-1}$  (Raman), 3064, 3057, 3042, 3040  $\text{cm}^{-1}$  computationally with PEDs 96% for the first two vibrations and 94% for the other two. The IR intensities are 7.61, 26.39, 9.71, 17.45 and the Raman activities are 171.49, 139.12, 103.12, 39.88 for these modes and 3095  $\text{cm}^{-1}$  (IR), 3091, 3057  $\text{cm}^{-1}$  (Raman), 3092 (PED 96%), 3079 (PED 99%), 3055 (PED 100%), 3047  $\text{cm}^{-1}$  (PED 96%) theoretically, with IR intensities 10.17, 5.34, 11.0, 13.51 and Raman activities 128.40, 139.32, 63.68, 73.11 respectively. The phenyl ring stretching modes are assigned at 1612, 1480, 1381, 1283  $\text{cm}^{-1}$  in the Raman spectrum, 1605-1283  $\text{cm}^{-1}$  theoretically for CMBAPC with a PED of 66% and 44% and 1610  $\text{cm}^{-1}$  in the IR spectrum, 1609, 1390, 1316  $\text{cm}^{-1}$  in the Raman spectrum, 1606-1315  $\text{cm}^{-1}$  theoretically for CMOBAPC and the PED values are 60% and 55%. The IR and Raman for these modes are 0.62, 19.32 and 97.60

and 23.18 for CMBAPC and 33.25, 39.57 and 103.38, 16.43 for CMOBAPC. The ring breathing mode is assigned for mono and 1,3-substituted benzenes, [74, 79] around  $1000\text{ cm}^{-1}$ . Ring breathing mode of mono and 1, 3-substituted benzenes is reported at  $1009\text{ cm}^{-1}$  [80] and  $972, 974\text{ cm}^{-1}$  [81]. The Ph ring breathing mode is at  $830\text{ cm}^{-1}$  (Raman),  $826\text{ cm}^{-1}$  (DFT) for CMBAPC and the PED is 68% with IR intensity 4.50 and Raman activity 34.92 and at  $832\text{ cm}^{-1}$  (Raman),  $831\text{ cm}^{-1}$  (DFT) for CMOBAPC with PED 42%, IR intensity 19.05 and Raman activity 28.89.

### 4.3 NMR spectra

The  $^1\text{H}$  and  $^{13}\text{C}$  NMR chemical shifts ( $\delta$ ) are simulated using the B3LYP functional with GIAO formalism using the cc-pVDZ basis sets. The simulated values are and are compared with the experimental chemical shifts provided in the table S2 of supplementary files [82]. For CMBAPC, the protons of the Ph and Pz rings resonate in the ranges, 7.4374 to 8.5528 ppm and 8.7571 ppm (simulation). The corresponding experimental shift are observed at 7.17-7.31 ppm and 8.33 ppm. In the case of CMOBAPC the corresponding values are, 6.8566-7.8029 ppm, 8.749 ppm (simulation), 6.85-7.33 ppm and 8.27 ppm (expt).  $\delta$  of the hydrogen atoms of the  $\text{CH}_2$  group are 4.0202, 7.8101 ppm (simulation) and 4.60 ppm (expt) for CMBAPC. CMOBAPC  $\delta$  are 4.3403, 5.1302 ppm (simulation) and 4.51 ppm (expt).  $\delta$  of the protons of the  $\text{CH}_3$  group are 2.1086, 2.866, 2.714 ppm (simulation) and 2.32 ppm (expt) for CMBAPC and for CMOBAPC the corresponding values are 4.134, 4.3683, 4.1193 ppm (simulation) and 3.72 ppm (expt). The  $\delta$  of the hydrogen atoms associated with nitrogen atoms are 5.7579 ( $\text{H}_{31}$ ), 8.3372 ( $\text{H}_{32}$ ), 5.7975 ( $\text{H}_{33}$ ) ppm (simulation) and 8.05, 8.46, 9.44 ppm (expt) for CMBAPC and for CMOBAPC the values are 7.9689 ( $\text{H}_{27}$ ), 5.6206 ( $\text{H}_{28}$ ), 8.4902 ( $\text{H}_{34}$ ), 8.34, 7.98, 9.34 ppm. High values are shown because of the presence of electronegative nitrogen atoms. In the present case,  $^{13}\text{C}$  NMR chemical shifts of the phenyl ring lie in the range 126.7819-138.5741 ppm for CMBAPC and in the range 108.7584-160.4545 ppm for CMOBAPC which are greater than 100 ppm as expected in literature. For the pyrazine ring the predicted  $\delta$  for CMBAPC is in the range 125.4737-149.7834 ppm and for CMOBAPC the range is 126.2343-149.9856 ppm. For other carbon atoms the predicted  $\delta$  are 119.0965 ppm ( $\text{C}_8$ ), 52.254 ppm ( $\text{C}_{11}$ ), 24.531 ppm ( $\text{C}_{24}$ ), 168.5289 ppm ( $\text{C}_{28}$ ) for CMBAPC and for CMOBAPC the corresponding values are 119.4674

(C<sub>8</sub>), 50.2523 (C<sub>11</sub>), 170.0456 (C<sub>24</sub>), 56.2693 (C<sub>30</sub>) ppm. For both the title compounds CMBAPC and CMOBAPC the predicted  $\delta$  agrees with the obtained results.

#### 4.4 Nonlinear optical properties

Compounds with non linear optical properties are very important in the design of high end electronic materials used for display and communication. The ability of a compound to show this property can be obtained from the hyperpolarisability data of the simulated Raman spectra of the compounds. The simulated polarizability values of CMBAPC and CMOBAPC are  $6.6472 \times 10^{-23}$  and  $7.3960 \times 10^{-23}$  esu. The first order hyperpolarizabilities are  $5.9414 \times 10^{-30}$  and  $5.9675 \times 10^{-30}$  esu for CMBAPC and CMOBAPC. It is in agreement with the reported analogues [65, 83]. The most interesting feature is that the values are 15.93 and 16.01 times with the property of urea, which is a standard NLO material [84]. The theoretically predicted second order hyperpolarizabilities are  $-17.889 \times 10^{-37}$  esu for CMBAPC and  $-20.027 \times 10^{-37}$  esu for CMOBAPC which are comparable with that of similar derivative [70]. Hence both compounds can be developed as possible materials with a potential to show non linear optical activities.

#### 4.5 Frontier Molecular Orbital analysis

Frontier molecular orbitals like HOMO and LUMO are very important in governing the reactivity preferences of any compound. For the compounds under the study, the pictures of the HOMO and LUMO are provided in the Fig.S3 of the supporting information. In CMBAPC, the HOMO is found to be spread over the entire molecule, except Ph ring and CH<sub>3</sub> group while in CMOBAPC, HOMO is over the entire molecule except Ph ring and OCH<sub>3</sub> group. The LUMO is delocalized over the pyrazine ring, C $\equiv$ N, C=O and NH<sub>2</sub> group for CMBAPC and CMOBAPC. The energy values of the FMO's can be used to get some interesting reactivity indices of the compounds. Ionization energy (I) and electron affinity (E) can be written as:  $I = -E_{\text{HOMO}}$ ,  $A = -E_{\text{LUMO}}$  [85]. Other parameters like hardness  $\eta$ , electronegativity  $\chi$  and chemical potential  $\mu$  can be written as:  $\eta = (I-A)/2$ ,  $\chi = (I+A)/2$  and  $\mu = -(I+A)/2$  [85]. The energy gap for CMBAPC and CMOBAPC are  $E_{\text{HOMO}} = -8.6213$  eV,  $E_{\text{LUMO}} = -6.1192$  eV, energy gap = 2.5021 eV. The I, A,  $\eta$ ,  $\mu$ ,  $\chi$  and global electrophilicity ( $\omega = \mu^2/2\eta$ ) for CMBAPC and CMOBAPC are 8.6213 eV, 6.1192 eV, 1.2511 eV, -7.3703 eV, 7.3703 eV, 21.710 eV respectively.

#### 4.6 Molecular Electrostatic Potential (MESP) analysis for reactivity

MESP is an important tool to predict the overall reactivity of a molecule towards reagents like nucleophiles and electrophiles. It identifies the charge regions of the molecules and provides the nature of such sites. This analysis is very much important for the prediction of biological activity of the molecules. The colour codes help to interpret the results in an easy manner. Red regions are more electronegative regions, which attract electrophiles, and blue regions are more electropositive, which attract more nucleophiles [86]. The general colour order is as follows - red < orange < yellow < green < blue [87]. In the MESP plot (Fig.S4- supporting information) for CMBAPC, red regions are over the C=O, C≡N and the Ph and for CMOBAPC, it is over the C=O, C≡N, Ph and OCH<sub>3</sub> group. Thus, there are both electrophilic and nucleophilic regions in the molecules, suggesting a high degree of reactivity and interaction towards polar media.

#### **4.7 Average Local Ionisation Energy (ALIE), Fukui functions and noncovalent interactions**

These functions also predict the reactivity of the atoms/groups towards charged reagents. ALIWE is used to predict the molecule sites which will be more prone to the attack of electrophilic reagents. If the ALIE values are small, electrons are more loosely bound, hence can be removed easily [88-91]. The ALIE diagram for the compounds CMBAPC and CMOBAPC molecules are provided in Fig.2 which indicate the ALIE values are almost same for both molecules. In cases of both molecules minimal ALIE values are located in the near vicinity of aromatic ring and nitrogen N6, suggesting these regions as possibly sensitive towards electrophilic attacks. These results are in accordance with our previously reported results regarding other pyrazine based molecules [92, 93]. In the present study the lowest ALIE values are somewhat near ~200 kcal/mol, while maximal ALIE ~370 kcal/mol. Study of density of electrons between atoms of title pyrazine molecules revealed formation of three and two intramolecular noncovalent interactions in the cases of CMBAPC and CMOBAPC, respectively. These noncovalent interactions are visualized and denoted in Fig.2, while strengths of these noncovalent interactions are provided in Table S3. The results in Table S3 suggest that the strongest noncovalent interaction formed in the case of CMOBAPC molecule, denoted with number 2 and with corresponding strength of  $-0.033$  electron/bohr<sup>3</sup>. Corresponding noncovalent

interaction in the case of CMBAPC has somewhat lower strength,  $-0.025$  electron/bohr<sup>3</sup>. The strength of noncovalent interaction marked with number 1 is somewhat higher in the case of CMBAPC comparing to CMOBAPC molecule. The third noncovalent interaction in the case of CMBAPC has weak strength of  $-0.007$  electron/bohr<sup>3</sup>.

In order to further search possibly important reactive sites we will refer to the results of Fukui functions [94]. In the cases of CMBAPC and CMOBAPC molecules, Fukui functions are presented in Fig.S5 (supporting information). In Fig.S5a, related to  $f^+$  function, there are several locations within the CMBAPC and CMOBAPC molecules characterized by the positive (purple) color, which indicates increase of electron density as a consequence of charge addition. In the case of CMBAPC the most intensive purple color is located in the near C2, while in the case of CMOBAPC the most intensive purple color is located in the near C24, designating these atoms as electrophilic after the addition of charge. On the other side in Fig.S5b, related to Fukui  $f^-$  function, for both molecules the most intensive red color, which determines positions where electron density decreases after the removal of charge, is located in the near oxygen atoms (O30 for CMBAPC and O25 for CMOBAPC) and cyano groups, designating these locations as nucleophilic after the removal of charge.

#### 4.8 Natural Bonding Orbital (NBO) analysis

NBO 3.1 version [95] implemented in the Gaussian 09 software package was used to generate output files required for the NBO studies. This study can lead light into the various type of hyperconjugative interactions possible in the molecules. In the case of CMBAPC, the hyperconjugative interactions are: C<sub>1</sub>-N<sub>6</sub> from C<sub>2</sub> of  $n_1(C_2) \rightarrow \pi^*(C_1-N_6)$ , C<sub>4</sub>-C<sub>5</sub> from N<sub>3</sub> of  $n_1(N_3) \rightarrow \sigma^*(C_4-C_5)$ , C<sub>4</sub>-C<sub>5</sub> from N<sub>6</sub> of  $n_1(N_6) \rightarrow \sigma^*(C_4-C_5)$ , C<sub>1</sub>-C<sub>8</sub> from N<sub>9</sub> of  $n_1(N_9) \rightarrow \sigma^*(C_1-C_8)$ , C<sub>28</sub>-N<sub>30</sub> from O<sub>29</sub> of  $n_2(O_{29}) \rightarrow \sigma^*(C_{28}-N_{30})$  and C<sub>28</sub>-O<sub>29</sub> from N<sub>30</sub> of  $n_1(N_{30}) \rightarrow \sigma^*(C_{28}-O_{29})$  with electron densities 0.45495, 0.04617, 0.04617, 0.03917, 0.05542 and 0.35616e and stabilization energies 103.12, 10.43, 9.42, 12.46, 21.39 and 71.53 kcal/mol. The stabilisation energy is highest for  $n_1(C_2) \rightarrow \pi^*(C_1-N_6)$ , and the value is more that 100 kcal/mol, which stabilises the molecule to a larger extend. Natural hybrid orbital  $n_2(O_{29})$ , occupy a higher energy orbital -0.26476 a.u with high degree of p-character (98.82%) and low occupation number (ON) 1.87291 and the other  $n_1(O_{29})$  occupy a lower energy orbital -0.69218a.u with p-character 38.53% and high ON1.97172.

In the case of CMOBAPC, the strong hyper-conjugative interactions observed are: C<sub>1</sub>-N<sub>6</sub> from C<sub>2</sub> of  $n_1(C_2) \rightarrow \sigma^*(C_1-N_6)$ , C<sub>4</sub>-N<sub>5</sub> from N<sub>3</sub> of  $n_1(N_3) \rightarrow \sigma^*(C_4-N_5)$ , C<sub>4</sub>-N<sub>5</sub> from N<sub>6</sub> of  $n_1(N_6) \rightarrow \sigma^*(C_4-C_5)$ , C<sub>1</sub>-C<sub>8</sub> from N<sub>9</sub> of  $n_1(N_9) \rightarrow \sigma^*(C_1-C_8)$ , C<sub>24</sub>-N<sub>26</sub> from O<sub>25</sub> of  $n_2(O_{25}) \rightarrow \sigma^*(C_{24}-N_{26})$ , C<sub>24</sub>-O<sub>25</sub> from N<sub>26</sub> of  $n_1(N_{26}) \rightarrow \sigma^*(C_{24}-O_{25})$ , C<sub>17</sub>-C<sub>19</sub> from O<sub>29</sub> of  $n_1(O_{29}) \rightarrow \sigma^*(C_{17}-C_{19})$  and C<sub>17</sub>-C<sub>19</sub> from O<sub>29</sub> of  $n_2(O_{29}) \rightarrow \pi^*(C_{17}-C_{19})$  with electron densities, 0.45475, 0.04618, 0.04618, 0.03918, 0.05543, 0.35615, 0.02726 and 0.38501e and stabilization energies, 103.05, 10.43, 9.42, 12.45, 21.39, 71.49, 6.85 and 28.21 kcal/mol. Here also, the highest stabilisation value is more than 100 kcal/mol indicating very high stability for the molecule. The NHO with higher energies, and low ON are  $n_2(O_{25})$  and  $n_2(O_{29})$  with energies, -0.26418, -0.30098a.u and p-characters, 98.83, 100% and ON, 1.87296 and 1.84950, but the orbitals with lower energies and high ON are,  $n_1(O_{25})$  and  $n_1(O_{29})$  with energies, -0.69170, -0.55367a.u and p-characters, 38.53, 58.76% and ON, 1.97172 and 1.96749. Thus, a very close to pure p-type lone pair orbital participates in the electron donation to the  $\sigma^*(C_1-N_6)$  orbital for  $n_1(C_2) \rightarrow \sigma^*(C_1-N_6)$ ,  $\sigma^*(C_4-C_5)$  orbital for  $n_1(N_3) \rightarrow \sigma^*(C_4-C_5)$ ,  $n_1(N_6) \rightarrow \sigma^*(C_4-C_5)$ ,  $\sigma^*(C_1-C_8)$  orbital for  $n_1(N_9) \rightarrow \sigma^*(C_1-C_8)$ ,  $\sigma^*(C_{24}-N_{26})$  orbital for  $n_2(O_{25}) \rightarrow \sigma^*(C_{24}-N_{26})$ ,  $\sigma^*(C_{24}-O_{25})$  orbital for  $n_1(N_{26}) \rightarrow \sigma^*(C_{24}-O_{25})$ ,  $\sigma^*(C_{17}-C_{19})$  orbital for  $n_1(O_{29}) \rightarrow \sigma^*(C_{17}-C_{19})$ , and  $\pi^*(C_{17}-C_{19})$  orbital for  $n_2(O_{29}) \rightarrow \pi^*(C_{17}-C_{19})$  interaction in the compound. The results provided in the Tables S4 and S5 (supporting information). The entire data shows that both molecules are highly stabilised by hyperconjugative interactions. This is having enormous effect on other physico-chemical and biological activity of the molecule.

#### 4.9 Autoxidation and hydrolysis studies

Oxidative degradation of organic pollutants, especially pharmaceutical ones, is considered to be one of the most important tools for their efficient removal from water resources. DFT calculations are particularly useful for the investigation of sensitivity towards oxidation [96-99]. Concerning the autoxidation mechanism, sensitivity of organic molecules towards this mechanism is related to the H-BDEs [24, 100, 101]. Interval of H-BDEs in range of 70 to 85 kcal/mol [102, 103] reflects high sensitivity towards autoxidation mechanism, while interval of H-BDEs between 85 to 90 kcal/mol reflects sensitivity towards autoxidation mechanism to low extent [103]. H-BDE values lower than 70 kcal/mol don't reflect at all sensitivity towards autoxidation mechanism [25, 102, 104]. Information about H-BDE values for CMBAPC and CMOBAPC molecules are provided in Fig.S6 (supporting information) and Table S6 (supporting

information). Calculated H-BDE values indicate that both CMBAPC and CMOBAPC molecules possess two hydrogen atoms (denoted with bond number 3 in Fig.S6) for which BDE value lies in the interval between 70 and 85 kcal/mol. Namely, BDE values for hydrogen atoms connected to carbon atom C12 for CMBAPC (C11 for CMOBAPC) are equal to ~84/82 kcal/mol, respectively. These H-BDE values indicate significant sensitivity towards autoxidation mechanism thanks to which pyrazine molecules investigated in this study might be prone to efficient degradation via oxidation. In this work we have also performed MD simulations in order to obtain an insight into the stability of title molecules in water. This was of particular importance since pharmacological molecules eventually end up in some type of water. After MD simulations we have calculated RDFs in order to see which atoms of molecules show any interactions with water molecules. RDFs of CMBAPC and CMOBAPC are provided in Fig.S7 (supporting information). According to the RDF results provided in Fig.S7 it can be concluded that both pyrazine derivatives investigated in this work have two H atoms with RDFs showing significant interactions with solvent water. Both of those hydrogen atoms belong to NH<sub>2</sub> group. However, although maximal  $g(r)$  values for these two atoms are located at distance lower than 2 Å, their maximal  $g(r)$  values are not so high, indicating that their interactions with water molecules after all are not so significant. Comparing CMBAPC and CMOBAPC it can be seen that CMOBAPC has somewhat stronger interactions with solvent, according to the interaction energy with solvent ( $E_{\text{int}}$ ) provided in Fig.S7, due to the presence of one more oxygen atom (O29) which has relatively significant RDF profile characterized with two solvation spheres.

#### 4.10 TD-DFT study on pyrazine derivatives molecule

In this study we have performed TD-DFT calculations to acquire UV spectra of the pyrazine derivatives and to analyze, thanks to the concept of natural transition orbitals (NTO) [105], which part of molecule's are the most important for the UV absorption. TD-DFT calculations also served us to investigate the charge transfer properties of pyrazine derivatives. In Fig.S8 (supporting information) we provide computationally obtained UV spectra of pyrazine derivatives investigated in this work. Both pyrazine derivatives investigated in this work have two specific absorption peaks at ~230 and ~370 nm, indicating that structural difference between them doesn't introduce significant changes when it comes to the light absorption properties. In Fig.S9 (supporting information) we are providing frontier molecular orbitals, and "particle" and

“hole” NTOs of the first excitation. In the case of CMBAPC (Fig.S9a) it can be seen that the first excitation “hole” and “particle” NTOs practically match the HOMO and LUMO orbitals, meaning that the first (and the lowest energy) excitation is mainly due to the HOMO to LUMO transition. However, this is not the case with CMOBAPC pyrazine derivative for which HOMO and the first excitation “hole” NTO do not fully match, while LUMO and the first excitation “particle” NTO match. After further inspection it was found that the first excitation “hole” NTO actually matches HOMO-1 orbital, indicating the importance of transition from HOMO-1 to LUMO orbital in the case of CMOBAPC pyrazine derivative. To analyze charge transfer within molecule using Multiwfn program [52-55] we have performed an analysis of the charge for the first excitation based on the electron density difference, according to the method described in [106]. Method provided in [106] is defined for charge transfer in one dimension, however in the implementation in Multiwfn program the method is generalized in three dimensions.

As introduced in [106] a quantity called charge transfer length (CT length) can be used for quantification of charge transfer. This quantity has been defined as a distance between barycenters of  $C_+$  and  $C_-$  functions. Definition of  $C_+$  and  $C_-$  functions relies on the electron density variation between the excited and the ground state and other important information on these functions can be seen in [106]. Before visualization of barycenters of positive and negative parts of  $C_+$  and  $C_-$  functions we are providing electron density variation due to the first excitation, Fig.S10 (supporting information). Green and blue colored area actually indicate where comes to the increase and decrease, respectively, in electron density as a consequence of excitation. According to the results presented in Fig.S10, as a consequence of the first excitation electron density changes mainly at ring containing nitrogen atoms and nitrogen atoms N9 and N10 (for both pyrazine derivatives). Electron density variation clearly emphasizes the importance of the aforementioned molecule part when it comes to the first excitation and is in accordance with the results obtained with NTOs. Namely, “particle” and “hole” NTOs of the first excitation (Figs.S9b and S9d) also emphasize the importance of the same part of molecule as electron density variation in Fig.S10 (supporting information). Further, we will refer to the barycenters of positive and negative parts of  $C_+$  and  $C_-$  functions, which are visualized in Fig.S11 (supporting information).  $C$  functions and their barycenters for title pyrazine derivatives indicate that CT length is  $\sim 1.57 \text{ \AA}$  for both molecules, initially suggesting that the excitation is of local type (LE),

meaning that holes and electrons share the same spatial range to high extent. However, since CT length is not significantly low to straightforwardly indicate LE type of excitation, we have also calculated the so called  $\Delta r$  coefficient, according to the paper [107], whose value also helps in identification of excitation type. It is suggested in the paper [107] that LE modes are characterized by  $\Delta r$  value lower than 2.0 Å. In the cases of pyrazine derivatives CMBAPC and CMOBAPC the following values for  $\Delta r$  index have been obtained: 1.36 Å and 0.66 Å, which clearly indicate a LE mode of excitation.  $\Delta r$  index has also been calculated by the Multiwfn program.

#### 4.11 Drug likeness

Drug likeness of newly synthesized title molecules has been assessed by calculation of well-known parameters which indicate the potential of some organic molecules to be considered as drug candidates. Lipinski's rule of five [108, 109] recognizes the values of some parameters to be considered active in humans. Moderately lipophilic character is desired, combined with HBD and HBA values lower than 5 and 10, respectively. In the same time mass should be lower than 500 u. Table S7 (supporting information) indicates that pyrazine derivatives CMBAPC and CMOBAPC fulfill all of these prerequisites. Ghose et al. [110] proposed that suitable drug candidate should possess molar refractivity. Number of rotatable bonds turned out also to be important parameter and Veber et al. [111] stated that for good oral bioavailability number of rotatable bonds should be lower than 10. This is also fulfilled by CMBAPC and CMOBAPC. It is also very important to emphasize that AlogP takes value lower than 3, which is very important for the "rule of three" defined by Congreve et al. [112], for the lead compounds in drug discovery.

#### 4.12 Molecular docking studies

Literature sources indicate that the pyrazine derivatives are extensively used in the anti-tubercular treatment [113], [114]. By the docking studies we want to make lucid whether the title compounds can act as ENR inhibitors. High resolution crystal structure of *Pseudomonas aeruginosa* Enoyl-Acyl carrier protein reductase (FabI) was downloaded from the RSCD protein data bank website with PDBID: 4NQZ [115]. Docking was done using Auto Dock Vina [116] and as reported in literature [117]. The candidate drug binds at the active site (Fig.3 and Fig.S12- supporting information) with the aid of weak non-covalent interactions. For the title

compounds CMBAPC, amino acid TYR149 shows hydrophobic  $\pi$ - $\pi$  stacked interaction with the phenyl ring, hydrophobic  $\pi$ -alkyl interaction with the phenyl ring and with carbon in the phenyl ring. For CMOBAPC amino acid ILE20, ALA21 and SER93 forms H-bond with N of C $\equiv$ N in the pyrazine ring, SER148 forms hydrogen bond with hydrogen of NH group, LYS166 shows carbon-hydrogen bond with oxygen of C=O in the pyrazine ring, ILE20 and LEU147 shows hydrophobic  $\pi$ -alkyl interaction with the pyrazine ring and ALA192 shows hydrophobic  $\pi$ -alkyl interaction with phenyl ring. The docked ligands form a stable complex with Enoyl-Acyl carrier protein reductase (FabI) and got binding affinity values of -6.7 kcal/mol for CMBAPC and -6.5 kcal/mol for CMOBAPC (Table 2). These results suggest that the title compounds might exhibit inhibitory activity against *Pseudomonas aeruginosa* Enoyl-Acyl carrier protein reductase (FabI).

## 5. Conclusion

The vibrational spectroscopic analysis of two cyanopyrazine-2-carboxamide derivatives, CMBAPC and CMOBAPC are carried out experimentally and theoretically and are found in close agreement. Using natural bond orbital analysis, stability of the title compounds arising from hyper conjugative interactions and charge delocalization have been analyzed. Compounds shows excellent NLO properties over the standard material urea. Molecular docking studies proves that the compounds exhibit inhibitory activity against *Pseudomonas aeruginosa* Enoyl-Acyl carrier protein reductase (FabI). ALIE surface shows that the benzene ring and nitrogen atoms N6 could be sensitive towards electrophilic attacks. Fukui functions showed the electrophilic character after the charge addition in the cases of carbon atoms C2 (CMBAPC) and C24 (CMOBAPC). H-BDE values showed that both of the pyrazine derivatives are sensitive towards autoxidation mechanism, thanks to the fact that two hydrogen atoms per each molecule have H-BDE values of  $\sim$ 83 kcal/mol. RDFs indicated that each pyrazine derivative have two hydrogen molecules with maximal  $g(r)$  values located at distances lower than 2 Å, however maximal  $g(r)$  values in these cases are relatively low, so it is not expected that these two molecules have significant interactions with water. TD-DFT calculations in combinations with NTOs and charge transfer analysis by Multiwfn program indicated the most important molecule sites for the lowest energy excitation. Electron density variation and the concepts of  $C_{+/-}$  functions and  $\Delta r$  parameter, indicated that the first excitation is of LE type.

## Acknowledgment

Part of this work has been performed thanks to the support received from Schrödinger Inc. Part of this study was conducted within the project supported by the Ministry of Education, Science and Technological Development of Serbia, grant numbers III41017.

## References

- [1] Y.S. Higasio, T. Shoji, Heterocyclic compounds such as pyrroles, pyridines, pyrrolidins, piperdines, indoles, imidazol and pyrazins, *Appl. Cataly. A: General* 221 (2001) 197-207.
- [2] R. Müller, S. Rappert, Pyrazines: occurrence, formation and biodegradation, *Appl. Microbiol. Biotechnol.* 85 (2010) 1315-1320.
- [3] J.A. Maga, C.E. Sizer, Pyrazines in foods, A review, *J. Agric. Food Chem.* 22(1) (1973) 22-30.
- [4] M. Asif, Piperazine and Pyrazine containing molecules and their diverse pharmacological activities, *Int. J. Adv. Sci. Res.*, 1 (2015) 5-11.
- [5] H. Tamioka, Current Status of Some Antituberculosis Drugs and the Development of new Antituberculous Agents with Special Reference to their In Vitro and In Vivo Antimicrobial Activities, *Curr. Pharm. Design* 12 (2006) 4047-4070.
- [6] V.B. Mathew, S.D. Arikatt, T.J. Sindhu, M. Chandran, A.R. Bhat, K. Krishnakumar, A review of Biological potential of pyrazine and related heterocyclic compounds, *World J. Pharm. Pharm. Sci.* 3 (2014) 1124-1132.
- [7] D. A. Mitchison, Pyrazine – on the antituberculosis drug frontline, *Natur. Med.* 2 (1996) 635-636.
- [8] S. Lin, S. Malkani, M. Lombardo, L. Yang, S.G. Mills, K. Chapman, J. Thompson, W.X. Zhang, R. Wang, R.M. Cubbon, E.A. O’neill, J.J. Hale, Design, synthesis, and biological evaluation of aminopyrazine derivatives as inhibitors of mitogen-activated protein kinase-activated protein kinase 2 (MK-2), *Bioorg. Med. Chem. Lett.* 25 (2015) 5402-5408.
- [9] H.H. Chen, A. Namil, B. Severns, J. Ward, C. Kelly, C. Drace, M.A. McLaughlin, S. Yacoub, B. Li, R. Patil, N. Sharif, M.R. Hellberg, A. Rusinko, I.H. Pang, K.D. Combrink, In vivo optimization of 2,3-diaminopyrazine Rho Kinase inhibitors for the treatment of glaucoma, *Bioorg. Med. Chem. Lett.* 24 (2014) 1875–1879.

- [10] T.I. El-Emary, Synthesis and Biological Activity of Some New Pyrazolo[3,4-b]Pyrazines, *J. Chin. Chem. Soc.* 53 (2006) 391-401.
- [11] M. Hamada, V. Roy, T.R. McBrayer, T. Whitaker, C. Urbina-Blanco, S.P. Nolan, J. Balzarini, R. Snoeck, G. Andrei, R.F. Schinazi, L.A. Agrofoglio, Synthesis and broad spectrum antiviral evaluation of bis(POM) prodrugs of novel acyclic nucleosides, *Eur. J. Med.Chem.* 67 (2013) 398-408.
- [12] M. Dolezal, J. Zitko, Pyrazine derivatives: a patent review (June 2012 – Present), *Expert Opinion on Therapeutic patents*, 25 (2015) 33 – 47.
- [13] L. Carlucci, G. Liani, D. M. Proserpie, A. Sironi, 1-, 2-, and 3-Dimensional Polymeric Frames in the Coordination Chemistry of AgBF<sub>4</sub> with Pyrazine. The First Example of Three Interpenetrating 3-Dimensional Triconnected Nets, *J. Am. Chem. Soc.* 117 (1995) 4562-4569.
- [14] S. Achelle, C. Baudequin, N. Ple, Luminescent materials incorporating pyrazine or quinoxaline moieties, *Dyes and Pigments*, 98 (2013) 575-600.
- [15] S. Deng, X. Li, H. Fu, Two pyrazine derivatives as inhibitors of the cold rolled steel corrosion in hydrochloric acid solution, *Corros. Sci.* 53 (2011) 822-828.
- [16] X. Li, S. Deng, H. Fu, Three pyrazine derivatives as corrosion inhibitors for steel in 1.0 M H<sub>2</sub>SO<sub>4</sub> solution, *Corros. Sci.* 53 (2011) 3241-3247.
- [17] M. Bouklah, A. Attayibat, S. Kertit, A. Ramdani, B. Hammouti, A pyrazine derivative as corrosion inhibitor for steel in sulphuric acid solution *Appl. Surf. Sci.* 242 (2005) 399-406.
- [18] S. Armaković, S. J. Armaković, J. P. Šetrajčić, I. J. Šetrajčić, Active components of frequently used  $\beta$ -blockers from the aspect of computational study, *J. Mol. Model.* 18(9) (2012) 4491-4501.
- [19] S. J. Armaković, S. Armaković, N. L. Finčur, F. Šibul, D. Vione, J. P. Šetrajčić, B. Abramović, Influence of electron acceptors on the kinetics of metoprolol photocatalytic degradation in TiO<sub>2</sub> suspension. A combined experimental and theoretical study, *RSC Adv.* 5(67) (2015) 54589-54604.
- [20] M. Blessy, R. D. Patel, P. N. Prajapati, Y. Agrawal, Development of forced degradation and stability indicating studies of drugs-A review, *J. Pharm. Anal.* 4(3) (2014) 159-165.

- [21] B. Abramović, S. Kler, D. Šojić, M. Laušević, T. Radović, D. Vione, Photocatalytic degradation of metoprolol tartrate in suspensions of two TiO<sub>2</sub>-based photocatalysts with different surface area. Identification of intermediates and proposal of degradation pathways, *J. Hazard. Mater.* 198 (2011) 123-132.
- [22] D.D. Četojević-Simin, S.J. Armaković, D.V. Šojić, B.F. Abramović, Toxicity assessment of metoprolol and its photodegradation mixtures obtained by using different type of TiO<sub>2</sub> catalysts in the mammalian cell lines, *Sci. Total Environ.* 463 (2013) 968-974.
- [23] J. A. War, K. Jalaja, Y.S. Mary, C.Y. Panicker, S. Armaković, S.J. Armaković, S.K. Srivastava, C. Van Alsenoy, Spectroscopic characterization of 1-[3-(1H-imidazol-1-yl)propyl]-3-phenylthiourea and assessment of reactive and optoelectronic properties employing DFT calculations and molecular dynamics simulations, *J. Mol. Struct.* 1129 (2017) 72-85.
- [24] S.W. Hovorka, C. Schöneich, Oxidative degradation of pharmaceuticals: theory, mechanisms and inhibition, *J. Pharm. Sci.* 90(3) (2001) 253-269.
- [25] P. Lienard, J. Gavartin, G. Boccardi, M. Meunier, Predicting drug substances autoxidation, *Pharm. Res.* 32(1) (2015) 300-310.
- [26] G.L. de Souza, L.M. de Oliveira, R.G. Vicari, A. Brown, A DFT investigation on the structural and antioxidant properties of new isolated interglycosidic O-(1→3) linkage flavonols, *J. Mol. Model.* 22(4) (2016) 1-9.
- [27] Z. Sroka, B. Żbikowska, J. Hładyszowski, The antiradical activity of some selected flavones and flavonols. Experimental and quantum mechanical study, *J. Mol. Model.* 21(12) (2015) 1-11.
- [28] H. Djeradi, A. Rahmouni, A. Cheriti, Antioxidant activity of flavonoids: a QSAR modeling using Fukui indices descriptors, *J. Mol. Model.* 20(10) (2014) 1-9.
- [29] S. Armaković, S.J. Armaković, S. Pelemiš, D. Mirjanić, Influence of sumanene modifications with boron and nitrogen atoms to its hydrogen adsorption properties, *Phys. Chem. Chem. Phys.* 18(4) (2016). 2859-2870.
- [30] M.J. Frisch, G.W. Trucks, H.B. Schlegel, G.E. Scuseria, M.A. Robb, J.R. Cheeseman, G. Scalmani, V. Barone, B. Mennucci, G.A. Petersson, H. Nakatsuji, M. Caricato, X. Li, H. P. Hratchian, A.F. Izmaylov, J. Bloino, G. Zheng, J.L. Sonnenberg, M. Hada, M. Ehara,

- K. Toyota, R. Fukuda, J. Hasegawa, M. Ishida, T. Nakajima, Y. Honda, O. Kitao, H. Nakai, T. Vreven, J.A. Montgomery, Jr., J.E. Peralta, F. Ogliaro, M. Bearpark, J.J. Heyd, E. Brothers, K.N. Kudin, V.N. Staroverov, T. Keith, R. Kobayashi, J. Normand, K. Raghavachari, A. Rendell, J.C. Burant, S.S. Iyengar, J. Tomasi, M. Cossi, N. Rega, J.M. Millam, M. Klene, J.E. Knox, J.B. Cross, V. Bakken, C. Adamo, J. Jaramillo, R. Gomperts, R.E. Stratmann, O. Yazyev, A.J. Austin, R. Cammi, C. Pomelli, J.W. Ochterski, R.L. Martin, K. Morokuma, V.G. Zakrzewski, G.A. Voth, P. Salvador, J.J. Dannenberg, S. Dapprich, A.D. Daniels, O. Farkas, J.B. Foresman, J.V. Ortiz, J. Cioslowski, D.J. Fox, Gaussian 09, Revision B.01, Gaussian, Inc., Wallingford CT, 2010.
- [31] J.B. Foresman, in: E. Frisch (Ed.), *Exploring Chemistry with Electronic Structure Methods: A Guide to Using Gaussian*, Gaussian Inc., Pittsburg, PA, 1996.
- [32] R. Dennington, T. Keith, J. Millam, Semichem Inc., Shawnee Mission KS, GaussView, Version 5, 2009.
- [33] J.M.L. Martin, C. Van Alsenoy, GAR2PED, A Program to Obtain a Potential Energy Distribution from a Gaussian Archive Record, University of Antwerp, Belgium, 2007.
- [34] *Materials Science Suite 2017-4*, Schrödinger, LLC, New York, NY. 2017.
- [35] A.D. Bochevarov, E. Harder, T.F. Hughes, J.R. Greenwood, D.A. Braden, D.M. Philipp, D. Rinaldo, M.D. Halls, J. Zhang, R.A. Friesner, Jaguar: A high-performance quantum chemistry software program with strengths in life and materials sciences, *Int. J. Quantum Chem.* 113(18) (2013) 2110-2142.
- [36] *Schrödinger Release 2017-4: MS Jaguar*, Schrödinger, LLC, New York, NY. 2017.
- [37] L.D. Jacobson, A.D. Bochevarov, M.A. Watson, T.F. Hughes, D. Rinaldo, S. Ehrlich, T.B. Steinbrecher, S. Vaitheeswaran, D.M. Philipp, M.D. Halls, Automated Transition State Search and Its Application to Diverse Types of Organic Reactions, *J. Chem. Theor. Comput.* 13(11) (2017) 5780-5797.
- [38] D. Shivakumar, J. Williams, Y. Wu, W. Damm, J. Shelley, W. Sherman, Prediction of absolute solvation free energies using molecular dynamics free energy perturbation and the OPLS force field, *J. Chem. Theor. Comput.* 6(5) (2010) 1509-1519.

- [39] Z. Guo, U. Mohanty, J. Noehre, T.K. Sawyer, W. Sherman, G. Krilov, Probing the  $\alpha$ -Helical Structural Stability of Stapled p53 Peptides: Molecular Dynamics Simulations and Analysis, *Chem. Biol. Drug Design*, 75(4) (2010) 348-359.
- [40] K.J. Bowers, E. Chow, H. Xu, R. O. Dror, M.P. Eastwood, B.A. Gregersen, J.L. Klepeis, I. Kolossvary, M.A. Moraes, F.D. Sacerdoti. Scalable algorithms for molecular dynamics simulations on commodity clusters. in SC 2006 Conference, Proceedings of the ACM/IEEE. 2006. IEEE.
- [41] V.B. Bregović, N. Basarić, K. Mlinarić-Majerski, Anion binding with urea and thiourea derivatives, *Coord. Chem. Rev.* 295 (2015) 80-124.
- [42] A.D. Becke, Density-functional thermochemistry. III. The role of exact exchange, *J. Chem. Phys.* 98(7) (1993). 5648-5652.
- [43] T. Yanai, D.P. Tew, N.C. Handy, A new hybrid exchange–correlation functional using the Coulomb-attenuating method (CAM-B3LYP), *Chem. Phys. Lett.* 393(1) (2004) 51-57.
- [44] Y. Cao, T. Hughes, D. Giesen, M.D. Halls, A. Goldberg, T.R. Vadicherla, M. Sastry, B. Patel, W. Sherman, A.L. Weisman, Highly efficient implementation of pseudospectral time-dependent density-functional theory for the calculation of excitation energies of large molecules, *J. Comput. Chem.* 37(16) (2016) 1425-1441.
- [45] E. Harder, W. Damm, J. Maple, C. Wu, M. Reboul, J.Y. Xiang, L. Wang, D. Lupyan, M.K. Dahlgren, J.L. Knight, OPLS3: a force field providing broad coverage of drug-like small molecules and proteins, *J. Chem. Theor. Comput.* 12(1) (2015) 281-296.
- [46] W.L. Jorgensen, D.S. Maxwell, J. Tirado-Rives, Development and testing of the OPLS all-atom force field on conformational energetics and properties of organic liquids, *J. Am. Chem. Soc.* 118(45) (1996) 11225-11236.
- [47] W.L. Jorgensen, J. Tirado-Rives, The OPLS [optimized potentials for liquid simulations] potential functions for proteins, energy minimizations for crystals of cyclic peptides and crambin, *J. Am. Chem. Soc.* 110(6) (1988) 1657-1666.
- [48] H.J. Berendsen, J.P. Postma, W.F. van Gunsteren, J. Hermans, Interaction models for water in relation to protein hydration, in *Intermolecular forces*. 1981, Springer. p. 331-342.

- [49] A. Otero-de-la-Roza, E.R. Johnson, J. Contreras-García, Revealing non-covalent interactions in solids: NCI plots revisited, *Phys. Chem. Chem. Phys.* 14(35) (2012) 12165-12172.
- [50] E.R. Johnson, S. Keinan, P. Mori-Sanchez, J. Contreras-Garcia, A.J. Cohen, W. Yang, Revealing noncovalent interactions, *J. Am. Chem. Soc.* 132(18) (2010) 6498-6506.
- [51] Schrödinger Release 2017-4: Maestro, Schrödinger, LLC, New York, NY. 2017.
- [52] T. Lu, F. Chen, Multiwfn: a multifunctional wavefunction analyzer, *J. Comput. Chem.* 33(5) (2012) 580-592.
- [53] T. Lu, F. Chen, Quantitative analysis of molecular surface based on improved Marching Tetrahedra algorithm, *J. Mol. Graphics Model.* 38 (2012) 314-323.
- [54] L. Tian, C. Feiwu, Calculation of molecular orbital composition, *Acta Chim. Sinica.* 69 (2011) 2393-2406.
- [55] M. Xiao, T. Lu, Generalized Charge Decomposition Analysis (GCDA) Method, *J. Adv. Phys. Chem.* 4 (2015) 111-124.
- [56] W. Humphrey, A. Dalke, K. Schulten, VMD: visual molecular dynamics, *J. Mol. Graphics*, 14(1) (1996) 33-38.
- [57] J.E. Stone, J. Gullingsrud, K. Schulten. A system for interactive molecular dynamics simulation. in *Proceedings of the 2001 symposium on Interactive 3D graphics.* 2001. ACM.
- [58] J. Eargle, D. Wright, Z. Luthey-Schulten, Multiple Alignment of protein structures and sequences for VMD, *Bioinformatics*, 22(4) (2006) 504-506.
- [59] D. Frishman, P. Argos, Knowledge-based protein secondary structure assignment, *Proteins: Struct. Funct. Bioinformatics*, 23(4) (1995) 566-579.
- [60] A. Varshney, J. F.P. Brooks, W. V. Wright, Linearly Scalable Computation of Smooth Molecular Surfaces, in *IEEE Computer Graphics and Applications*, 1994.
- [61] M.F. Sanner, A.J. Olson, J.-C. Spehner. Fast and robust computation of molecular surfaces. in *Proceedings of the eleventh annual symposium on Computational geometry.* 1995. ACM.

- [62] R. Sharma, M. Zeller, V.I. Pavlovic, T.S. Huang, Z. Lo, S. Chu, Y. Zhao, J.C. Phillips, K. Schulten, Speech/gesture interface to a visual-computing environment. *IEEE Computer Graphics and Applications*, 2000. 20(2): p. 29-37.
- [63] J.E. Stone, An efficient library for parallel ray tracing and animation. 1998, Masters Theses, [http://scholarsmine.mst.edu/masters\\_theses/1747](http://scholarsmine.mst.edu/masters_theses/1747).
- [64] Y.S. Mary, A. A. Saadi, K. Haruna, R. Thomas, Roxy M S, S. Popoola, V. Santhosh. Conformational profile, vibrational assignments, NLO properties and molecular docking of biologically active herbicide 1,1-dimethyl-3-phenylure. *Heliyon*, 5, 6 (2019), e01987 DOI: <https://doi.org/10.1016/j.heliyon.2019.e01987>
- [65] J. Lukose, C.Y. Panicker, P.S. Nayak, B. Narayana, B.K. Sarojini, C. Van Alsenoy, A.A. Al-Saadi, Synthesis, structural and vibrational investigation on 2-phenyl-N-(pyrazin-2-yl)acetamide combining XRD diffraction, FT-IR and NMR spectroscopies with DFT calculations, *Spectrochim. Acta*. 135 (2015) 608-616.
- [66] W. He, G. Zhou, J. Li, A. Tian, Molecular design of analogues of 2, 6-diamino-3, 5-dinitropyrazine-1-oxide, *J. Mol. Struct. Theochem*. 668 (2004) 201-208.
- [67] H. Takeuchi, M. Sato, T. Tsuji, H. Takashima, T. Egawa, S. Konaka, *J. Mol. Struct.* 485-486 (1999) 175-181.
- [68] S.M. Bakalova, A.G. Santos, I. Timcheva, J. Kaneti, I.L. Filipova, G.M. Dobrikov, V.D. Dimitrov, Electronic absorption and emission spectra and computational studies of some 2-aryl, 2-styryl, and 2-(4'-aryl)butadienyl quinazolin-4-ones, *J. Mol. Struct. Theochem*. 710 (2004) 229-234.
- [69] E.D. Stevens, Low-temperature experimental electron density distribution of formamide, *Acta. Cryst.* 34B (1978) 544-551.
- [70] S.H.R. Sebastian, M.A. Al-Alshaikh, A.A. El-Emam, C.Y. Panicker, J. Zitko, M. Dolezal, C. Van Alsenoy, Spectroscopic, quantum chemical studies, Fukui functions, in vitro antiviral activity and molecular docking of 5-chloro-N-(3-nitrophenyl) pyrazine-2-carboxamide, *J. Mol. Struct.* 1119 (2016) 188-199.
- [71] M. Barthes, G. De Nunzio, M. Ribet, Polarons or proton transfer in chains of peptide groups ?, *Synth. Met.* 76 (1996) 337-340.

- [72] K. Tamagawa, T. Iijima, M. Kimura, Molecular structure of benzene, *J. mol. Struct.* 30 (1976) 243-253.
- [73] K.B. Borizenko, C. W. Bock, I. Hargittai, Molecular Geometry of Benzaldehyde and Salicylaldehyde: A Gas-Phase Electron Diffraction and ab Initio Molecular Orbital Investigation, *J. Phys. Chem.* 100 (1996) 7426-7434.
- [74] N.P.G. Roeges, *A Guide to the Complete Interpretation of Infrared Spectra of Organic Structures*, John Wiley and Sons Inc., New York, 1994.
- [75] R.M. Silverstein, G.C. Bassler, T.C. Morrill, *Spectrometric Identification of Organic Compounds*, fifth ed., John Wiley and Sons Inc., Singapore, 1991.
- [76] N.B. Colthup, L.H. Daly, S.E. Wiberly, *Introduction of Infrared and Raman Spectroscopy*, Academic Press, New York, 1975.
- [77] L.J. Bellamy, *The Infrared Spectrum of Complex Molecules*, third ed., Chapman and Hall, London, 1975.
- [78] J. Coates, *Encyclopedia of Analytical Chemistry*, in: R.A. Meyers (Ed.), *Interpretation of Infrared Spectrum, A Practical Approach*, John Wiley and Sons Ltd., Chichester, 2000.
- [79] G. Varsanyi, *Assignments of Vibrational Spectra of Seven Hundred Benzene Derivatives*, Wiley, New York, 1974.
- [80] A.S. El-Azab, K. Jalaja, A.A.M. Abdel-Aziz, A.M. Al-Obaid, Y.S. Mary, C.Y. Panicker, C. Van Alsenoy, Spectroscopic analysis (FT-IR, FT-Raman and NMR) and molecular docking study of ethyl 2-(4-oxo-3-phenethyl-3,4-dihydroquinazolin-2-ylthio)-acetate, *J. Mol. Struct.* 1119 (2016) 451-461.
- [81] Y.S. Mary, K. Raju, C.Y. Panicker, A.A. Al-Saadi, T. Thiemann, Molecular conformational analysis, vibrational spectra, NBO analysis and first hyperpolarizability of (2E)-3-(3-chlorophenyl)prop-2-enoic anhydride based on density functional theory calculations, *Spectrochim. Acta* 131 (2014) 471-483.
- [82] K. Wolinski, J.F. Hinton, P. Pulay, Efficient implementation of the gauge independent atomic orbital method for NMR chemical shift calculations, *J. Am. Chem. Soc.* 112 (1990) 8251-8260.
- [83] Y.S. Mary, C.Y. Panicker, R. Thomas, B. Narayana, S. Samshuddin, B.K. Sarojini, S. Armaković, S. J. Armaković, G. G. Pillai, Theoretical studies on the structure and various

- physico-chemical and biological properties of a terphenyl derivative with immense anti-protozoan activity. *Polycyclic Aromatic Compounds* (2019).  
<https://doi.org/10.1080/10406638.2019.1624974>
- [84] C. Adant, M. Dupuis, J.L. Bredas, Ab initio study of the nonlinear optical properties of urea, electron correlation and dispersion effects, *Int. J. Quantum Chem.* 56 (2004) 497-507.
- [85] R.G. Parr, R.G. Pearson, Absolute hardness, companion parameter to absolute electronegativity, *J. Am. Chem. Soc.* 105 (1983) 7512-7516.
- [86] A.M. Koster, M. Leboeuf, D.R. Salahub, Molecular Electrostatic Potentials from Density Functional Theory, *Theor. Comput. Chem.* 3 (1996) 105-142.
- [87] D. Majumdar, S. Das, R.Thomas, Z. Ullah, S. S. Sreejith, D. Das, K. Bankura, D. Mishra, Syntheses, X-ray crystal structures of two new Zn(II)-dicyanamide complexes derived from H<sub>2</sub>vanen-type compartmental ligands: Investigation of thermal, photoluminescence, in vitro cytotoxic effect and DFT-TDDFT studies. *Inorganica Chimica Acta* 492 (2019): 221-234 <https://doi.org/10.1016/j.ica.2019.04.041>
- [88] J.S. Murray, J.M. Seminario, P. Politzer, P. Sjoberg, Average local ionization energies computed on the surfaces of some strained molecules, *Int. J. Quantum Chem.* 38(S24) (1990) 645-653.
- [89] P. Politzer, F. Abu-Awwad, J.S. Murray, Comparison of density functional and Hartree-Fock average local ionization energies on molecular surfaces, *Int. J. Quantum Chem.* 69(4) (1998) 607-613.
- [90] F.A. Bulat, A. Toro-Labbé, T. Brinck, J.S. Murray, P. Politzer, Quantitative analysis of molecular surfaces: areas, volumes, electrostatic potentials and average local ionization energies, *J. Mol. Model.* 16(11) (2010) 1679-1691.
- [91] P. Politzer, J.S. Murray, F.A. Bulat, Average local ionization energy: a review, *J. Mol. Model.* 16(11) (2010) 1731-1742.
- [92] S. Beegum, Y.S. Mary, H.T. Varghese, C.Y. Panicker, S. Armaković, S.J. Armaković, J. Zitko, M. Dolezal, C. Van Alsenoy, Vibrational spectroscopic analysis of cyanopyrazine-2-carboxamide derivatives and investigation of their reactive properties by DFT calculations and molecular dynamics simulations, *J. Mol. Struct.* 1131 (2017) 1-15.

- [93] P.K. Ranjith, E.S. Al-Abdullah, F.A.M. Al-Omary, A.A. El-Emam, P.L. Anto, Y.S. Mary, S. Armaković, S.J. Armaković, J. Zitko, M. Dolezal, C. Van Alsenoy, FT-IR and FT-Raman characterization and investigation of reactive properties of N-(3-iodo-4-methylphenyl)pyrazine-2-carboxamide by molecular dynamics simulations and DFT calculations. *J. Mol. Struct.* 1136 (2017) 14-24.
- [94] A. Michalak, F. De Proft, P. Geerlings, R. Nalewajski, Fukui functions from the relaxed Kohn-Sham orbitals, *J. Phys. Chem.A*, 103(6) (1999) 762-771.
- [95] E. D. Glendening, A.E. Reed, J.E. Carpenter, F. Weinhold, NBO Version 3.1, TCI, University of Wisconsin, Madison, 1998
- [96] X. Ren, Y. Sun, X. Fu, L. Zhu, Z. Cui, DFT comparison of the OH-initiated degradation mechanisms for five chlorophenoxy herbicides, *J. Mol. Model.* 19(6) (2013) 2249-2263.
- [97] L.-l. Ai, J.-y. Liu, Mechanism of OH-initiated atmospheric oxidation of E/Z-CF<sub>3</sub>CF=CFCF<sub>3</sub>: a quantum mechanical study, *J. Mol. Model.* 20(4) (2014) 1-10.
- [98] W. Sang-aroon, V. Amornkitbamrung, V. Ruangpornvisuti, A density functional theory study on peptide bond cleavage at aspartic residues: direct vs cyclic intermediate hydrolysis, *J. Mol. Model.* 19(12) (2013) 5501-5513.
- [99] J. Kieffer, É. Brémond, P. Lienard, G. Boccardi, In silico assessment of drug substances chemical stability, *J. Mol. Struct. THEOCHEM*, 954(1) (2010) 75-79.
- [100] K.A. Connors, G.L. Amidon, V.J. Stella, *Chemical stability of pharmaceuticals: a handbook for pharmacists*, 1986: John Wiley & Sons.
- [101] D. Johnson, L. Gu, Autoxidation and antioxidants, *Encycl. Pharm. Technol.* 1 (1988) 415-449.
- [102] J.S. Wright, H. Shadnia, L.L. Chepelev, Stability of carbon-centered radicals: Effect of functional groups on the energetics of addition of molecular oxygen, *J. Comput. Chem.* 30(7) (2009) 1016-1026.
- [103] G. Gryn'ova, J.L. Hodgson, M.L. Coote, Revising the mechanism of polymer autooxidation, *Org.Biomol. Chem.* 9(2) (2011) 480-490.
- [104] T. Andersson, A. Broo, E. Evertsson, Prediction of Drug Candidates' Sensitivity Toward Autoxidation: Computational Estimation of C-H Dissociation Energies of Carbon-Centered Radicals, *J. Pharm. Sci.* 103(7) (2014) 1949-1955.

- [105] R.L. Martin, Natural transition orbitals, *J. Chem. Phys.* 118(11) (2003) 4775-4777.
- [106] T. Le Bahers, C. Adamo, I. Ciofini, A qualitative index of spatial extent in charge-transfer excitations, *J. Chem. Theor. Comput.* 7(8) (2011) 2498-2506.
- [107] C.A. Guido, P. Cortona, B. Mennucci, C. Adamo, On the metric of charge transfer molecular excitations: A simple chemical descriptor, *J. Chem. Theor. Comput.* 9(7) (2013) 3118-3126.
- [108] C.A. Lipinski, F. Lombardo, B.W. Dominy, P.J. Feeney, Experimental and computational approaches to estimate solubility and permeability in drug discovery and development settings, *Adv. Drug Delivery Rev.* 23(1-3) (1997) 3-25.
- [109] C.A. Lipinski, Lead-and drug-like compounds: the rule-of-five revolution, *Drug Discovery Today: Technologies*, 1(4) (2004) 337-341.
- [110] A.K. Ghose, V.N. Viswanadhan, J.J. Wendoloski, A knowledge-based approach in designing combinatorial or medicinal chemistry libraries for drug discovery. 1. A qualitative and quantitative characterization of known drug databases, *J. Combinat. Chem.* 1(1) (1999) 55-68.
- [111] D.F. Veber, S.R. Johnson, H.-Y. Cheng, B.R. Smith, K.W. Ward, K.D. Kopple, Molecular properties that influence the oral bioavailability of drug candidates, *J. Med. Chem.* 45(12) (2002) 2615-2623.
- [112] M. Congreve, R. Carr, C. Murray, H. Jhoti, A 'rule of three' for fragment-based lead discovery?, *Drug Discover. Today*, 8(19) (2003) 876-877.
- [113] L.E. Seitz, W.J. Suling, R.C. Reynolds, Synthesis and antimycobacterial activity of pyrazine and quinoxaline derivatives, *J. Med. Chem.* 45(25) (2002) 5604-5606.
- [114] X. He, A. Alian, R.M. Stroud, P.R. Otriz de Montellano, Pyrrolidine carboxamides as a novel class of inhibitors of enoyl acyl carrier protein reductase from *Mycobacterium tuberculosis*, *J. Med. Chem.* (2006) 6308-6323.
- [115] J.H. Lee, A.K. Park, Y.M. Chi, S.W. Jeong, Crystal Structures of *Pseudomonas aeruginosa* Enoyl-ACP Reductase (FabI) in the presence an Absence of NAD<sup>+</sup> and Triclosan, *Bull. Korean Chem. Soc.* 36 (2015) 322- 326.

- [116] O. Trott, A. J. Olson, AutoDock Vina: improving the speed and accuracy of docking with a new scoring function, efficient optimization, J. Comput. Chem. 31 (2010) 455-461.
- [117] B. Kramer, M. Rarey, T. Lengauer, Evaluation of the FLEXX incremental construction algorithm for protein ligand docking, Proteins: Struct. Funct. Genet. 37 (1999) 228-241.

### Figure Captions

Scheme

- Fig.1 Optimized geometry of 5-cyano-3-((4-methylbenzyl)amino)pyrazine-2-carboxamide (CMBAPC) and 5-cyano-3-((4-methoxybenzyl)amino)pyrazine-2-carboxamide (CMOBAPC)
- Fig.2 ALIE surface of (a) 5-cyano-3-((4-methylbenzyl)amino)pyrazine-2-carboxamide (CMBAPC) and (b) 5-cyano-3-((4-methoxybenzyl)amino)pyrazine-2-carboxamide (CMOBAPC)
- Fig.3 The docked ligands 5-cyano-3-((4-methylbenzyl)amino)pyrazine-2-carboxamide (CMBAPC) and 5-cyano-3-((4-methoxybenzyl)amino)pyrazine-2-carboxamide (CMOBAPC) at the active site of Enoyl-Acyl carrier protein reductase

Table 1

Table 1.1

Calculated (scaled wave numbers), observed IR, Raman bands and assignments of 5-cyano-3-((4-methylbenzyl)amino)pyrazine-2-carboxamide (CMBAPC)

B3LYP/CC-pVDZ (5D, 7F)		IR	Raman	Assignments <sup>a</sup>
$\nu(\text{cm}^{-1})$	$\text{IR}_I$	$R_A$	$\nu(\text{cm}^{-1})\nu(\text{cm}^{-1})$	-
3572	87.73	84.99	- 3578	$\nu\text{NH}_2(99)$
3425	63.06	163.74	3447 3423	$\nu\text{NH}_2(99)$
3293	187.24	132.77	3259 3293	$\nu\text{NH}(99)$
3076	3.50	148.33	3088 3080	$\nu\text{CHI}(99)$
3064	7.61	171.49	- -	$\nu\text{CHII}(96)$
3057	26.39	139.12	3051 3057	$\nu\text{CHII}(96)$
3042	9.71	103.12	- -	$\nu\text{CHII}(94)$
3040	17.45	39.88	3021 3037	$\nu\text{CHII}(94)$
2995	15.00	72.42	- 2994	$\nu\text{CH}_3(100)$
2966	15.73	113.79	- 2968	$\nu\text{CH}_3(100)$
2963	6.01	86.45	- -	$\nu\text{CH}_2(99)$
2910	34.86	278.30	- 2905	$\nu\text{CH}_3(60)$
2893	38.66	165.32	2865 2887	$\nu\text{CH}_2(100)$
2257	2.19	536.23	2238 2262	$\nu\text{C}\equiv\text{N}(89)$
1682	419.40	37.67	1688 1681	$\nu\text{C}=\text{O}(60), \nu\text{CN}(14)$
1605	0.62	97.60	- 1612	$\nu\text{PhII}(66)$
1572	469.66	5.41	- 1566	$\nu\text{CN}((26), \delta\text{NH}(17), \nu\text{PhI}(16))$
1561	62.81	3.77	- -	$\nu\text{PhII}(60), \nu\text{PhI}(13)$
1523	118.40	210.73	1530 1533	$\nu\text{PhI}(58), \nu\text{PhII}(16)$
1501	236.50	17.10	1506 1506	$\delta\text{NH}_2(61), \nu\text{CN}(12)$
1488	3.08	1.24	- 1480	$\delta\text{CHII}(12), \nu\text{PhII}(44), \nu\text{CC}(11)$
1484	247.21	36.82	- -	$\nu\text{PhI}(40), \nu\text{CN}(14), \delta\text{CHI}(11)$
1434	11.97	15.29	1424 1435	$\nu\text{PhI}(41), \delta\text{CHI}(44)$
1421	25.63	11.21	- -	$\delta\text{CH}_2(90)$

1414	21.28	12.95	1402	1412	$\delta\text{CH}_3(65)$ , $\delta\text{CH}_2(21)$
1399	5.34	18.05	-	-	$\delta\text{CH}_3(98)$
1381	4.64	7.56	-	1381	$\nu\text{PhII}(42)$ , $\delta\text{CH}_3(44)$
1361	24.14	79.83	1354	1361	$\nu\text{CC}(19)$ , $\delta\text{NH}_2(11)$ , $\nu\text{PhI}(11)$
1342	0.48	37.60	-	-	$\delta\text{CH}_3(86)$
1331	56.17	16.63	13321	1333	$\delta\text{CH}_2(68)$
1305	24.29	25.89	1303	1308	$\delta\text{NH}(49)$ , $\nu\text{PhII}(10)$
1283	19.32	23.18	-	1283	$\nu\text{PhII}(44)$ , $\delta\text{CH}_2(42)$
1268	55.16	44.86	1264	1267	$\delta\text{CHII}(43)$ , $\nu\text{PhI}(13)$ , $\delta\text{CH}_2(10)$
1257	148.84	62.68	-	-	$\nu\text{PhI}(51)$
1228	28.24	9.07	1234	1230	$\nu\text{PhI}(50)$ , $\delta\text{CHI}(18)$
1199	30.92	33.34	1184	1194	$\delta\text{CH}_2(63)$
1188	6.80	16.94	-	-	$\nu\text{CC}(44)$ , $\nu\text{PhII}(28)$
1183	9.40	19.85	-	-	$\nu\text{CC}(40)$ , $\delta\text{CHII}(19)$ , $\nu\text{PhII}(13)$
1180	69.49	6.70	-	1181	$\nu\text{PhI}(30)$ , $\delta\text{CHI}(17)$
1149	4.77	7.07	-	1153	$\delta\text{CHII}(82)$
1098	2.07	28.77	-	1097	$\nu\text{CN}(41)$ , $\nu\text{PhI}(48)$
1088	7.89	10.17	1077	1079	$\delta\text{CHII}(50)$ , $\nu\text{PhII}(22)$
1050	0.26	29.27	-	-	$\delta\text{NH}_2(50)$ , $\nu\text{CN}(39)$
1034	4.18	2.35	1045	1039	$\nu\text{CN}(45)$
1015	0.35	0.10	-	-	$\delta\text{PhI}(29)$ , $\delta\text{CN}(16)$
1010	4.30	0.28	1019	1012	$\delta\text{CH}_3(62)$ , $\gamma\text{CHII}(13)$
992	10.25	0.23	-	991	$\delta\text{CHII}(52)$ , $\nu\text{PhII}(40)$
962	8.83	2.51	964	965	$\delta\text{CH}_3(59)$ , $\delta\text{CH}_2(10)$
946	0.42	1.85	-	949	$\gamma\text{CHII}(70)$
942	2.65	1.96	935	-	$\gamma\text{CHII}(54)$ , $\delta\text{CH}_2(13)$
919	5.80	4.40	-	916	$\gamma\text{CHII}(56)$ , $\delta\text{CH}_2(23)$
848	9.40	0.28	-	844	$\gamma\text{CHI}(82)$
826	4.50	34.92	-	830	$\nu\text{PhII}(68)$ , $\nu\text{CC}(14)$
823	0.05	4.60	-	-	$\gamma\text{CHII}(100)$

800	7.19	3.14	-	-	$\tau$ PhI(42), $\gamma$ CC(19), $\gamma$ C=O(12)
791	16.74	5.56	777	783	$\gamma$ CHII(100)
770	3.27	1.78	-	-	$\nu$ CC(16), $\tau$ PhI(20), $\delta$ PhII(19)
717	9.60	14.55	-	-	$\tau$ PhII(39), $\delta$ PhI(32)
715	18.57	0.71	-	-	$\tau$ PhI(38), $\gamma$ C=O(26), $\gamma$ CC(13)
700	14.37	0.91	-	-	$\tau$ PhII(50), $\gamma$ CC(13)
693	49.29	1.12	693	693	$\tau$ PhII(25), $\gamma$ NH(43)
670	37.96	3.71	-	672	$\delta$ PhI(32), $\nu$ CC(18), $\delta$ C=O(16)
663	7.90	1.67	-	-	$\gamma$ CN(30), $\gamma$ CC(27), $\tau$ PhI(18)
628	0.28	6.59	629	632	$\delta$ PhII(80)
605	3.20	3.71	-	-	$\tau$ NH <sub>2</sub> (58)
603	4.58	4.46	601	601	$\tau$ NH <sub>2</sub> (44), $\delta$ CC(19), $\delta$ PhI(18)
595	2.19	5.27	-	-	$\delta$ CC(32), $\delta$ PhI(12), $\delta$ NH <sub>2</sub> (10)
536	1.97	2.68	542	528	$\delta$ C=O(33), $\delta$ PhI(10)
506	23.89	0.85	503	509	$\gamma$ CC(34), $\tau$ PhII(25)
496	13.31	2.84	-	-	$\tau$ PhI(28), $\gamma$ CN(16), $\gamma$ CC(11)
494	6.81	1.16	-	493	$\tau$ PhI(37), $\gamma$ CN(10)
461	3.05	3.39	477	466	$\gamma$ CC(24), $\tau$ PhII(21), $\delta$ PhII(19)
415	8.54	2.32	409	411	$\delta$ CC(33), $\tau$ PhI(39)
406	25.50	2.43	-	-	$\tau$ PhI(37), LC $\equiv$ N(24), $\gamma$ CC(21)
401	0.86	0.05	-	397	$\tau$ PhII(83)
346	0.50	2.34	-	-	$\delta$ CC(56)
337	1.39	3.59	-	-	$\delta$ PhI(34), $\delta$ C=O(10)
300	1.18	4.36	-	309	$\gamma$ CC(49), $\tau$ PhI(17)
281	98.86	1.69	-	-	$\gamma$ NH <sub>2</sub> (63)
272	7.04	1.36	-	273	$\delta$ CC(60)
252	47.45	1.08	-	-	$\gamma$ CC(33), $\gamma$ NH <sub>2</sub> (21), $\tau$ PhI(18)
212	4.25	0.77	-	-	$\delta$ CC(41), LC $\equiv$ N(18)
198	4.05	1.09	-	195	$\delta$ CH <sub>2</sub> (14), $\delta$ CN(13), $\delta$ CC(11)
169	5.67	0.34	-	171	$\tau$ PhI(18), $\gamma$ NH(17), $\gamma$ CC(12)

130	3.15	2.19	-	-	$\delta$ CC(23), LC $\equiv$ N(16), $\tau$ PhII(14)
124	5.62	1.07	-	122	$\gamma$ NH(20), $\tau$ CN(16), $\tau$ PhII(13)
95	1.24	2.77	-	-	$\delta$ CN(27), LC $\equiv$ N(16), $\tau$ PhII(11)
76	0.19	0.40	-	83	$\tau$ C=O(67), $\gamma$ NH <sub>2</sub> (17)
65	3.40	1.39	-	-	$\tau$ PhI(58), $\tau$ CN(11), $\gamma$ CC(15)
39	0.39	0.24	-	-	$\tau$ CH <sub>3</sub> (64), $\gamma$ CC(16)
34	1.00	4.77	-	-	$\gamma$ NH(26), $\tau$ CH <sub>3</sub> (15), $\delta$ CH <sub>2</sub> (10)
16	0.43	6.48	-	-	$\tau$ CC(51), $\tau$ CN(14)
12	0.07	8.52	-	-	$\tau$ CN(61), $\tau$ CC(12)

<sup>a</sup> $\nu$ -stretching;  $\delta$ -in-plane deformation;  $\gamma$ -out-of-plane deformation;  $\tau$ -torsion; PhI-phenyl ring; PhII-pyrazine ring.

**Table 1.2**

Calculated (scaled wave numbers), observed IR, Raman bands and assignments of 5-cyano-3-((4-methoxybenzyl)amino)pyrazine-2-carboxamide (CMOBAPC)

B3LYP/CC-pVDZ (5D, 7F)		IR	Raman	Assignments <sup>a</sup>	
$\nu(\text{cm}^{-1})$	IR <sub>I</sub>	R <sub>A</sub>	$\nu(\text{cm}^{-1})$	$\nu(\text{cm}^{-1})$	
				-	
3573	87.07	85.08	-	-	$\nu$ NH <sub>2</sub> (99)
3425	62.16	163.38	3389	3436	$\nu$ NH <sub>2</sub> (99)
3296	186.93	129.67	3297	3294	$\nu$ NH(99)
3092	10.17	128.40	3095	3091	$\nu$ CHII(96)
3079	5.34	139.32	-	-	$\nu$ CHII(99)
3076	3.59	150.20	-	3057	$\nu$ CHI(99)
3055	11.00	63.68	-	3057	$\nu$ CHII(100)
3047	13.51	73.11	-	-	$\nu$ CHII(96)
3017	23.03	158.71	3020	3020	$\nu$ CH <sub>3</sub> (91)
2972	5.03	80.46	2970	2970	$\nu$ CH <sub>2</sub> (100)
2948	39.51	70.81	2944	2940	$\nu$ CH <sub>3</sub> (100)
2895	41.13	165.77	-	2893	$\nu$ CH <sub>2</sub> (100)
2885	63.28	163.05	-	2880	$\nu$ CH <sub>3</sub> (100)

2257	2.39	541.06	2245	2247	$\nu\text{C}\equiv\text{N}(89)$
1682	410.17	38.90	1686	1684	$\nu\text{C}=\text{O}(60)$
1606	33.25	103.39	1610	1609	$\nu\text{PhII}(60), \delta\text{CHII}(11)$
1571	524.17	13.59	1574	1570	$\nu\text{CN}(25), \delta\text{NH}(43)$
1565	59.90	5.44	-	-	$\nu\text{PhII}(59)$
1522	112.89	211.96	1527	1525	$\nu\text{PhI}(58)$
1501	235.36	17.75	1505	1504	$\delta\text{NH}_2(61), \nu\text{CN}(12)$
1489	54.90	2.27	-	-	$\nu\text{PhII}(34), \delta\text{CHII}(37)$
1483	311.85	38.72	-	-	$\nu\text{PhI}(40), \delta\text{CHI}(11)$
1434	10.92	16.74	1434	1437	$\nu\text{PhI}(41), \delta\text{CHI}(44)$
1423	10.40	11.82	-	-	$\delta\text{CH}_2(85)$
1421	61.23	9.48	-	-	$\delta\text{CH}_3(83)$
1405	6.29	22.90	1408	-	$\delta\text{CH}_3(95)$
1403	11.36	7.50	-	-	$\delta\text{CH}_3(82)$
1395	0.97	5.44	-	1390	$\nu\text{PhII}(44), \delta\text{CHII}(25)$
1362	27.15	86.43	1359	-	$\nu\text{CC}(19), \delta\text{NH}_2(11), \nu\text{PhII}(11)$
1334	116.61	27.09	-	1338	$\delta\text{CH}_2(64), \nu\text{PhII}(11)$
1315	39.57	16.43	-	1316	$\nu\text{PhII}(55)$
1286	28.39	39.47	1284	1284	$\delta\text{CH}_2(69), \nu\text{PhI}(14)$
1266	36.79	29.99	1270	-	$\delta\text{CHII}(59)$
1258	157.64	74.01	1260	1260	$\nu\text{PhI}(53)$
1239	299.74	23.90	1240	1238	$\nu\text{CO}(39), \nu\text{PhII}(28)$
1228	27.78	8.73	-	-	$\nu\text{PhI}(50), \delta\text{CHI}(18)$
1195	63.24	22.38	-	-	$\delta\text{CH}_2(62)$
1184	9.86	30.34	-	-	$\nu\text{CC}(41), \nu\text{PhII}(11)$
1180	66.23	6.56	1182	1180	$\nu\text{PhI}(30), \delta\text{CHI}(16), \delta\text{CH}_2(10)$
1149	5.29	4.37	-	-	$\delta\text{CH}_3(75)$
1139	49.20	7.66	-	1136	$\delta\text{CHII}(78)$
1114	0.86	2.49	1117	-	$\delta\text{CH}_3(93)$
1094	4.11	33.21	1096	-	$\nu\text{CN}(44), \nu\text{PhI}(46), \nu\text{CC}(10)$

1082	9.69	3.27	-	-	$\delta$ CHII(63), $\nu$ PhII(22)
1050	0.37	29.20	1055	1057	$\delta$ NH <sub>2</sub> (54), $\nu$ CN(38)
1032	40.80	3.89	-	-	$\nu$ CO(65)
1029	26.45	3.89	1027	1031	$\nu$ CN(37), $\nu$ CO(10)
1013	0.89	0.28	-	1009	$\delta$ PhI(29), $\nu$ CC(10)
982	3.07	0.12	-	-	$\delta$ CHII(48), $\nu$ PhII(33)
941	0.78	2.59	954	-	$\gamma$ CHII(73)
934	9.35	5.60	928	930	$\delta$ CH <sub>2</sub> (31), $\gamma$ CHII(38)
910	4.91	3.55	-	-	$\gamma$ CHII(63), $\delta$ CH <sub>2</sub> (11), $\tau$ PhII(11)
847	9.22	0.29	-	-	$\gamma$ CHI(82)
831	19.05	28.89	-	832	$\gamma$ CHII(17), $\nu$ PhII(42)
813	16.29	14.91	814	815	$\gamma$ CH <sub>2</sub> (54), $\gamma$ CO(11)
799	7.44	3.07	-	-	$\tau$ PhI(42), $\gamma$ CN(18), $\gamma$ C=O(12)
794	8.89	3.15	791	-	$\gamma$ CHII(84)
772	5.87	2.02	769	770	$\delta$ CN(18), $\delta$ PhII(38)
719	7.37	12.05	-	-	$\tau$ PhII(34)
714	15.80	0.60	-	-	$\tau$ PhI(38), $\gamma$ C=O(27), $\gamma$ CC(14)
703	6.08	1.93	-	-	$\tau$ PhII(51), $\gamma$ CO(11)
690	53.45	0.79	692	693	$\tau$ CN(34), $\gamma$ NH(39), $\tau$ PhII(11)
669	38.79	4.35	-	670	$\delta$ PhI(33), $\delta$ C=O(16)
662	9.82	1.73	-	-	$\gamma$ CN(30), $\gamma$ CC(26), $\tau$ PhI(17)
624	0.88	7.25	628	628	$\delta$ PhII(72)
605	5.32	4.17	-	-	$\tau$ NH <sub>2</sub> (59), $\tau$ PhI(18)
602	7.31	4.63	601	603	$\delta$ PhI(18), $\tau$ NH <sub>2</sub> (47), $\delta$ CC(15)
595	4.68	5.11	-	-	$\delta$ CN(23), $\delta$ CC(20)
544	2.22	2.97	-	-	$\delta$ C=O(21), $\gamma$ CO(10)
518	23.04	0.57	522	-	$\gamma$ CO(21), $\tau$ PhII(20), $\gamma$ CC(13)
512	9.13	3.80	-	-	$\delta$ CO(26), $\delta$ PhII(11)
495	17.37	1.33	-	-	$\tau$ PhI(44), $\gamma$ CN(22), $\gamma$ CC(14)
485	3.24	3.01	487	487	$\delta$ CN(31), LC $\equiv$ N(19)

429	2.56	2.40	-	-	$\delta\text{CO}(25)$ , $\tau\text{PhII}(17)$ , $\delta\text{PhII}(12)$
417	12.83	2.66	-	-	$\delta\text{CN}(23)$ , $\tau\text{PhII}(12)$ , $\delta\text{PhII}(11)$
408	1.79	1.19	-	-	$\tau\text{PhII}(71)$
405	23.76	2.51	405	407	$\tau\text{PhI}(36)$ , $\text{LC}\equiv\text{N}(22)$ , $\gamma\text{CC}(20)$
338	0.97	3.65	-	340	$\delta\text{PhI}(36)$ , $\delta\text{C}=\text{O}(12)$
325	2.67	3.91	-	320	$\gamma\text{CC}(21)$ , $\delta\text{CC}(17)$ , $\tau\text{PhII}(19)$
305	2.37	0.87	-	-	$\delta\text{CN}(33)$ , $\delta\text{CO}(16)$ , $\delta\text{CC}(15)$
279	96.45	1.79	-	-	$\gamma\text{NH}_2(62)$ , $\tau\text{PhI}(16)$
256	22.68	1.82	-	260	$\gamma\text{CC}(12)$ , $\tau\text{CH}_3(22)$ , $\delta\text{CC}(12)$
248	33.10	0.85	-	-	$\gamma\text{CC}(25)$ , $\tau\text{CH}_3(11)$ , $\tau\text{PhI}(11)$
238	2.18	0.44	-	232	$\tau\text{CH}_3(54)$ , $\tau\text{PhI}(20)$
201	2.31	0.39	-	-	$\delta\text{CC}(17)$ , $\tau\text{PhII}(13)$ , $\delta\text{CO}(11)$
188	4.45	1.86	-	-	$\delta\text{CO}(25)$ , $\text{LC}\equiv\text{N}(11)$
167	2.75	0.32	-	164	$\tau\text{PhI}(20)$ , $\text{LC}\equiv\text{N}(15)$ , $\gamma\text{NH}(14)$
138	7.31	1.06	-	-	$\tau\text{CO}(24)$ , $\tau\text{PhII}(23)$ , $\delta\text{CC}(16)$
121	3.75	1.67	-	119	$\gamma\text{NH}(18)$ , $\tau\text{CN}(14)$ , $\tau\text{C}=\text{O}(12)$
100	1.49	2.51	-	-	$\tau\text{CO}(20)$ , $\delta\text{CC}(17)$
79	2.18	1.94	-	-	$\tau\text{CO}(39)$ , $\tau\text{CH}_3(15)$ , $\tau\text{C}=\text{O}(10)$
79	0.64	0.57	-	-	$\tau\text{C}=\text{O}(61)$ , $\gamma\text{NH}_2(16)$
65	3.29	1.35	-	-	$\tau\text{PhI}(58)$ , $\gamma\text{CC}(15)$ , $\tau\text{CN}(11)$
32	0.99	5.90	-	-	$\gamma\text{NH}(34)$ , $\tau\text{CN}(20)$
17	0.83	8.36	-	-	$\tau\text{CC}(66)$ , $\gamma\text{CC}(15)$
7	0.11	3.64	-	-	$\tau\text{CN}(58)$ , $\delta\text{CH}_2(11)$ , $\delta\text{CN}(10)$

<sup>a</sup> $\nu$ -stretching;  $\delta$ -in-plane deformation;  $\gamma$ -out-of-plane deformation;  $\tau$ -torsion; PhI-phenyl ring; PhII-pyrazine ring.

Table 2

the binding affinity values of different poses of the title compounds predicted by Autodock Vina.

**Table 2.1 - CMBAPC**

Mode	Affinity (kcal/mol)	Distance from best mode (Å)	
		RMSD l.b.	RMSD u.b.
-	-		
1	-6.7	0.000	0.000
2	-6.6	2.384	2.926
3	-6.6	2.362	2.851
4	-6.2	4.919	7.906
5	-6.1	2.942	3.929
6	-6.1	4.537	8.074
7	-6.1	2.441	3.858
8	-6.1	1.916	3.004
9	-6.1	1.868	2.991

**Table 2.2 - CMOBAPC**

Mode	Affinity (kcal/mol)	Distance from best mode (Å)	
		RMSD l.b.	RMSD u.b.
-	-		
1	-6.5	0.000	0.000
2	-6.3	2.947	6.471
3	-6.3	13.640	16.605
4	-6.3	2.479	2.857
5	-6.2	1.865	2.508

6	-6.2	14.137	16.371
7	-6.2	15.115	18.079
8	-6.2	14.640	16.913
9	-6.0	6.019	9.213

Journal Pre-proof

## Highlights

- Reports spectral analysis and computational studies of two new cyanopyrazine-2-carboxamide derivatives
- Details physico-chemical property studies attempted.
- Compounds shows excellent NLO property
- Docking results suggests about activity towards *Pseudomonas aeruginosa* Enoyl-Acyl carrier protein reductase

Journal Pre-proof

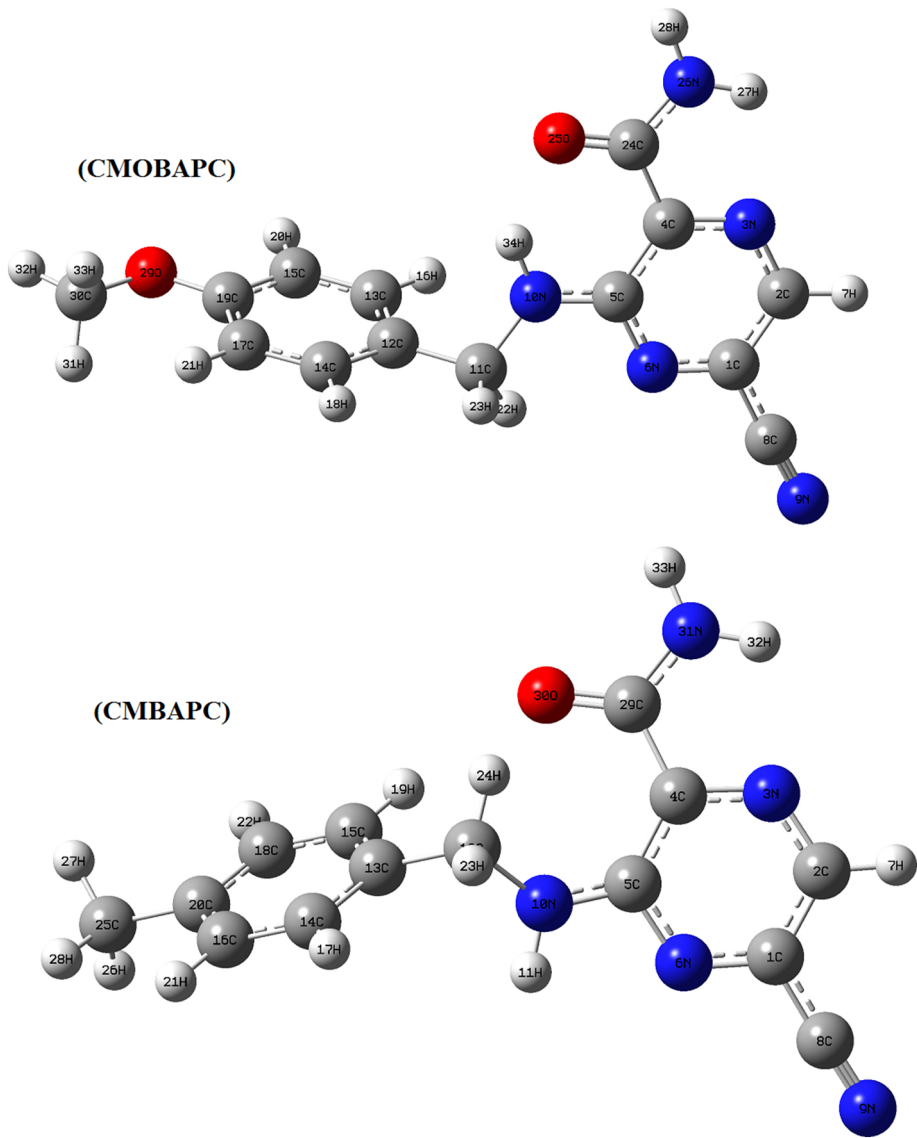
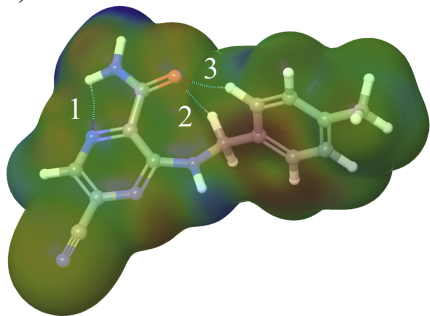


Figure 1

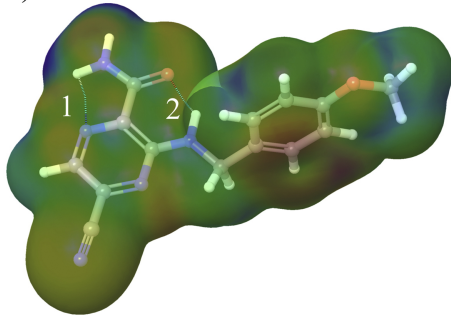
a)



min: 201.99

max: 368.80

b)



min: 201.61

max: 369.75

ALIE [kcal/mol]

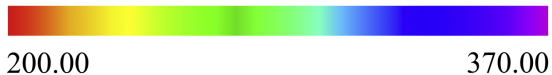
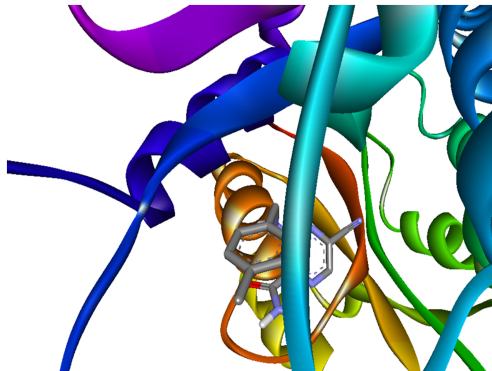
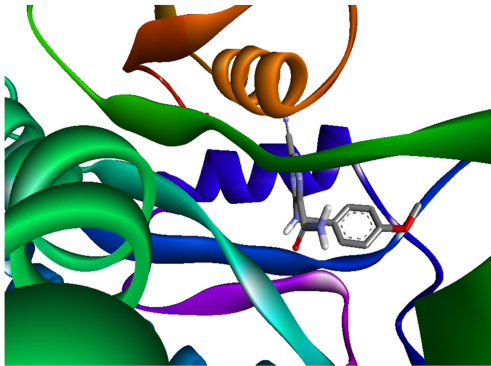


Figure 2



(CMBAPC)



(CMOBAPC)

Figure 3